

FINAL
CONTRACT REPORT

**PROOF TESTING
A BRIDGE DECK DESIGN
WITH GLASS FIBER REINFORCED
POLYMER BARS AS TOP MAT
OF REINFORCEMENT**

JASON K. CAWRSE
Graduate Research Engineer

CARIN L. ROBERTS-WOLLMANN
Assistant Professor

Via Department of Civil and Environmental Engineering
Virginia Polytechnic Institute & State University



VIRGINIA TRANSPORTATION RESEARCH COUNCIL

Standard Title Page - Report on State Project

Report No. VTRC 03-R15	Report Date June 2003	No. Pages 67	Type Report: Final	Project No.: 60807
				Contract No.
Title: Proof Testing a Bridge Deck Design with Glass Fiber Reinforced Polymer Bars as Top Mat of Reinforcement				Key Words: Glass fiber reinforced polymer (GFRP), reinforcement, bridge deck, structural design
Authors: Jason K. Cawrse and Carin L. Roberts-Wollmann				
Performing Organization Name and Address: Virginia Transportation Research Council 530 Edgemont Road Charlottesville, VA 22903				
Sponsoring Agencies' Name and Address Virginia Department of Transportation 1401 E. Broad Street Richmond, VA 23219				
<p>Abstract</p> <p>The primary objective of this project was to test a full-scale prototype of a bridge deck design containing glass fiber reinforced polymer (GFRP) bars as the top mat of reinforcement. The test deck mimics the design of the deck of one span of the new bridge over Gills Creek on Rt. 668 in Franklin County, Virginia. The purpose of the tests was to verify the deck design and provide assurance that the deck will behave as expected. Aspects of the behavior of the bridge deck, such as failure load, failure mode, cracking load, crack widths, deflections, and internal stresses, were examined. Four tests were performed on the deck, all of which tested the deck in negative moment regions. The tests comprised two overhang tests, one test of the deck over an interior girder, and one test of a cantilever section of the composite deck and girder. The cantilever test modeled the deck in a continuous bridge over an interior support. From the tests, it was concluded that the design of the deck was quite conservative.</p> <p>The secondary objectives of this project were to comment on the construction of a bridge deck reinforced with GFRP bars, note the advantages and disadvantages, and critique the current state of the art of designing bridge decks with GFRP reinforcement. It was found that the advantages of construction with GFRP bars easily outweighed the disadvantages and that the placing of the top mat of GFRP bars was much easier than the placing of the bottom mat of steel bars.</p> <p>The state of the art for the design of bridge decks reinforced with GFRP bars was found to be generally conservative. Three primary criteria dictate the deck design: strength, allowable stresses in the GFRP bars, and crack widths. For this deck, the size and spacing of the transverse GFRP bars were governed by crack control criteria. In testing the deck, however, it was found that the measured crack widths were far smaller than the calculated widths. The measured bar stresses, after cracking, were below those calculated, and below the allowable for all but the cantilever test. The ultimate failure loads were between 3.7 and 7.6 times the design wheel load plus impact. All failures were due to punching shear and were between 91% and 149% of the predicted failure load. Current methods for calculating one-way shear grossly under-predicted capacity.</p> <p>The current design is safe and should prove to be low maintenance. Improvements in design approach, particularly for crack widths and one-way shear, could result in more economical designs in the future. Although current methods for calculating strength and serviceability requirement do not result in accurate predictions of behavior, they do result in conservative designs.</p>				

FINAL CONTRACT REPORT

**PROOF TESTING A BRIDGE DECK DESIGN
WITH GLASS FIBER REINFORCED POLYMER BARS
AS TOP MAT OF REINFORCEMENT**

J. K. Cawrse
Graduate Research Engineer

C. L. Roberts-Wollmann, Ph.D., P.E.
Assistant Professor

**Via Department of Civil and Environmental Engineering
Virginia Polytechnic Institute and State University**

Project Manager

Michael C. Brown, Ph.D., P.E., Virginia Transportation Research Council

Contract Research Sponsored by the
Virginia Transportation Research Council

Virginia Transportation Research Council
(A Cooperative Organization Sponsored Jointly by the
Virginia Department of Transportation and
the University of Virginia)

Charlottesville, Virginia

June 2003
VTRC 03-CR15

NOTICE

The project that is the subject of this report was done under contract for the Virginia Department of Transportation, Virginia Transportation Research Council. The contents of this report reflect the views of the authors, who are responsible for the facts and the accuracy of the data presented herein. The contents do not necessarily reflect the official views or policies of the Virginia Department of Transportation, the Commonwealth Transportation Board, or the Federal Highway Administration. This report does not constitute a standard, specification, or regulation.

Each contract report is peer reviewed and accepted for publication by Research Council staff with expertise in related technical areas. Final editing and proofreading of the report are performed by the contractor.

Copyright 2003 by the Commonwealth of Virginia.

ABSTRACT

The primary objective of this project was to test a full-scale prototype of a bridge deck design containing glass fiber reinforced polymer (GFRP) bars as the top mat of reinforcement. The test deck mimics the design of the deck of one span of the new bridge over Gills Creek on Rt. 668 in Franklin County, Virginia. The purpose of the tests was to verify the deck design and provide assurance that the deck will behave as expected. Aspects of the behavior of the bridge deck, such as failure load, failure mode, cracking load, crack widths, deflections, and internal stresses, were examined. Four tests were performed on the deck, all of which tested the deck in negative moment regions. The tests comprised two overhang tests, one test of the deck over an interior girder, and one test of a cantilever section of the composite deck and girder. The cantilever test modeled the deck in a continuous bridge over an interior support. From the tests, it was concluded that the design of the deck was quite conservative.

The secondary objectives of this project were to comment on the construction of a bridge deck reinforced with GFRP bars, note the advantages and disadvantages, and critique the current state of the art of designing bridge decks with GFRP reinforcement. It was found that the advantages of construction with GFRP bars easily outweighed the disadvantages and that the placing of the top mat of GFRP bars was much easier than the placing of the bottom mat of steel bars.

The state of the art for the design of bridge decks reinforced with GFRP bars was found to be generally conservative. Three primary criteria dictate the deck design: strength, allowable stresses in the GFRP bars, and crack widths. For this deck, the size and spacing of the transverse GFRP bars were governed by crack control criteria. In testing the deck, however, it was found that the measured crack widths were far smaller than the calculated widths. The measured bar stresses, after cracking, were below those calculated, and below the allowable for all but the cantilever test. The ultimate failure loads were between 3.7 and 7.6 times the design wheel load plus impact. All failures were due to punching shear and were between 91% and 149% of the predicted failure load. Current methods for calculating one-way shear grossly under-predicted capacity.

The current design is safe and should prove to be low maintenance. Improvements in design approach, particularly for crack widths and one-way shear, could result in more economical designs in the future. Although current methods for calculating strength and serviceability requirement do not result in accurate predictions of behavior, they do result in conservative designs.

FINAL CONTRACT REPORT

**PROOF TESTING A BRIDGE DECK DESIGN
WITH GLASS FIBER REINFORCED POLYMER BARS
AS TOP MAT OF REINFORCEMENT**

J. K. Cawrse
Graduate Research Engineer

C.L. Roberts-Wollmann
Assistant Professor

**Via Department of Civil and Environmental Engineering
Virginia Polytechnic Institute and State University**

INTRODUCTION

Reinforced concrete structures in the United States are deteriorating at an alarming rate. The estimated cost to fix these structures is between \$1 and \$3 trillion. Highway bridges are one such concrete structure and have an estimated repair cost of \$50 billion. In fact, it has been reported that “over one-quarter of all bridges in the United States are either deficient or obsolete” with damaged bridge decks being the leading reason (Bedard 1992).

The primary reason for this structural deficiency is corrosion of the steel reinforcement within the concrete. This corrosion results in a large increase in the volume of the metal, which in turn causes internal stresses in the concrete, which can cause cracking and spalling of the concrete (Bradberry 2001). In concrete bridge decks, this corrosion is primarily due to either exposure to harsh environments such as high humidity climates and salt-water environments or direct application of de-icing salts and chemicals to the bridge deck (Khalifa et al. 1993).

Many approaches are available to attempt to prevent this corrosion in bridge decks. They include increased concrete cover, coated steel bars, concrete penetrating sealants, de-icing management, galvanized steel bars, stainless steel bars, cathodic protection systems, and concrete admixtures (Bradberry 2001). Another approach is the use of composite fiber-reinforced polymer (FRP) reinforcing bars, which have excellent corrosion resistance. FRP composites have been around for years, initially used in the aerospace industry and then adopted by many other industries such as the automobile and sporting goods industries. The high costs of these composites may initially seem unreasonable, but when compared with the additional costs of the aforementioned methods such as the additional material price, construction time, maintenance, etc., the costs are comparable to that of epoxy-coated steel (Bedard 1992).

These bars have many properties that differ significantly from those of steel bars. Some of these differences can be viewed as advantageous and some can be viewed as disadvantageous. On the positive side, they are very lightweight, high strength, and are non-reactive to chlorides. However, their modulus of elasticity is significantly lower than that of steel and their stress-strain behavior is linearly elastic up to failure, unlike steel, which has a yield plateau to warn of

failure. Because of these properties, many engineers and researchers believe that it will be most efficient to use the FRP bars as only the top mat of reinforcement in bridge decks and continue to use steel as the bottom mat.

The Virginia Department of Transportation (VDOT) has recently decided to replace a bridge on Rt. 668 over Gills Creek in Franklin County that is outdated and structurally deficient. The new bridge will consist of three simple spans, one of which will use glass fiber reinforced polymer (GFRP) reinforcing bars as the top mat of reinforcement and epoxy-coated mild steel as the bottom mat of reinforcement in the deck. The design for the deck containing the GFRP bars was accomplished using the *Guide for the Design and Construction of Concrete Reinforced with FRP Bars* (ACI 2001) in conjunction with the properties and recommendations reported by DeFreese (2001) in his thesis, which investigated GFRP bars produced by three different manufacturers.

PURPOSE AND SCOPE

The primary objective of this project was to build and test a full-scale prototype of the deck of the Rt. 668 bridge over Gills Creek, which uses GFRP bars as top mat reinforcement. This is to verify the deck design and to provide VDOT engineers with assurance the deck will not have unexpected problems due to the use of this new material. Within this scope, the level of conservatism of the design is addressed and the behavior of the bridge and deck is examined. The aspects of behavior that were examined are failure load, failure mode, cracking load, crack widths, deflections, and internal stresses. The behavior of the bridge deck at service loads and at ultimate load was examined.

To accomplish these objectives, a full-scale prototype of the bridge deck was constructed in the Virginia Tech Structures and Materials Laboratory. The deck was instrumented with strain gauges on various GFRP and steel reinforcing bars, and wire displacement potentiometers (wire pots) were attached to the deck and girders at designated locations to measure deflections. Four different load tests were then performed on the bridge deck. Each test placed the GFRP bars in tension: two tests of the overhangs, one test of a negative moment region over an interior girder, and one test to mimic a composite girder continuous over an interior support. Data for each test were recorded using a data acquisition system, and the deck was inspected at various load increments for cracks and crack widths. Finally, the data were reduced, analyzed, and compared to calculated theoretical values.

The secondary objectives of the project were to comment on the construction of a bridge deck reinforced with GFRP bars, note any concerns or possible advantages in the construction process, and critique the state of the art of designing bridge decks that use FRP reinforcement. To accomplish the evaluation, as the prototype bridge deck was constructed by the researchers, observations and comments on the construction were noted. To critique the state of the art of designing these decks, design procedures and guidelines were reviewed and used in the analysis of the data.

METHODS

Bridge Prototype

The prototype of the bridge was built to full scale with a few modifications. Table 1 shows a comparison between the prototype bridge deck and the actual bridge deck design. The prototype is three girders wide with an overhang on each side whereas the actual bridge is six girders wide with an overhang on each side. The overall width of the prototype bridge deck is 17 ft 4 in and the length is 24 ft. The deck also has four 1 ft by 2 ft block outs, two on either side, to accommodate the columns for a load frame as shown in Figure 1.

Table 1. Bridge Deck Design Comparison

	Prototype Bridge Deck	Actual Bridge Deck
Overall width	17 ft 4 in	30 ft 4 in
Overall length	24 ft	45 ft
No. of spans/type	3/continuous	1/simple
No. of girders	3	5
Type of girder	W27x94	W27x94
Spacing between girders	6 ft 6 in	6 ft 6 in
No. of overhangs	2	2
Width of overhangs	2 ft 2 in	2 ft 2 in
Top mat reinforcement	GFRP	GFRP
Bottom mat reinforcement	bare steel	epoxy-coated steel
Top mat transverse bar size	No. 5	No. 6
Top mat longitudinal bar size	No. 6	No. 6
Bottom mat transverse bar size	No. 6	No. 6
Bottom mat longitudinal bar size	No. 4	No. 4
Minimum concrete strength	4000 psi	4000 psi
Slab depth between girders	7.5 in	8.0 in ¹
Overhang slab depth	8.5 in	9.0 in ¹

¹ includes ½ in sacrificial wearing surface.

Deck Design

The design of the deck was accomplished using the loads, load factors, load combinations, impact factors, and effective slab widths as prescribed by the American Association of State Highway and Transportation Officials (AASHTO)(1998). The design of the GFRP reinforced one-way slab was based on the recommendations in the *Guide for the Design and Construction of Concrete Reinforced with FRP Bars* (ACI 2001). The design criteria included three ultimate limit states, flexural strength, one-way shear strength, and two-way shear strength, and three serviceability checks, allowable stress in the GFRP bars, crack widths, and deflections. The deck was designed as a one-way slab supported on pin supports at the girders. The wheel patch load multiplied by the impact factor was divided by the effective slab width to determine a load per foot width of slab. The overhangs also were designed for an impact to the top of the barrier rail. The design of the transverse reinforcing was dictated by the crack control criteria.

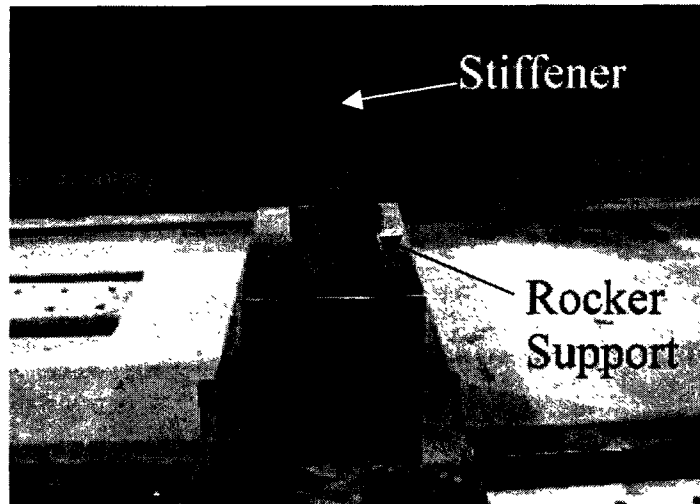


Figure 2. Rocker support.

Reinforcing Bars

The top mat of reinforcement for the deck consisted of GFRP bars. The design called for epoxy-coated mild steel in the bottom mat; however, bare steel was used since, for a short-term lab project, corrosion is not an issue. The steel bars were No. 6 in the transverse direction and No. 4 in the longitudinal direction. The GFRP bars used were manufactured by Hughes Brothers, Inc. and are denoted by a helical wrap and a mild sand impregnation. The design called for No. 6 GFRP bars in both the longitudinal and transverse directions. However, smaller diameter bars were used in the prototype to account for the fact that GFRP bars lose strength with time in a concrete environment.

ACI (2001) recommends that GFRP bars in concrete exposed to earth and weather have an environmental reduction factor, CE, of 0.7 applied to their guaranteed tensile strength to yield the design tensile strength. The design tensile strength, f_{tu} , is the estimated tensile strength of the bar after 50 years. The area of a No. 5 bar (0.31 in^2) is approximately equal to 70% of the area of a No. 6 bar (0.44 in^2). Therefore, No. 5 transverse bars were used in the prototype to model the strength of the transverse bars in the actual bridge after 50 years of service.

Steel Reinforcement Layout

The No. 6 mild steel bars were spaced 8 in on center in the transverse direction, as shown in Figure 4. The clear cover over the bottom bars of the slab was 1 in between girders and 2 in on the overhangs. The longitudinal No. 4 steel bars were laid on top of the transverse bars. The spacing of the longitudinal bars varied and is illustrated in Figure 5.

GFRP Reinforcement Layout

The No. 5 GFRP bars were spaced 4 in on center in the transverse direction, as shown in Figure 4. The depth to the center of the bars was 2 in everywhere except the east half of the north overhang, where the depth was $2\frac{1}{8}$ in. An attempt was made to increase the depth to $2\frac{1}{2}$

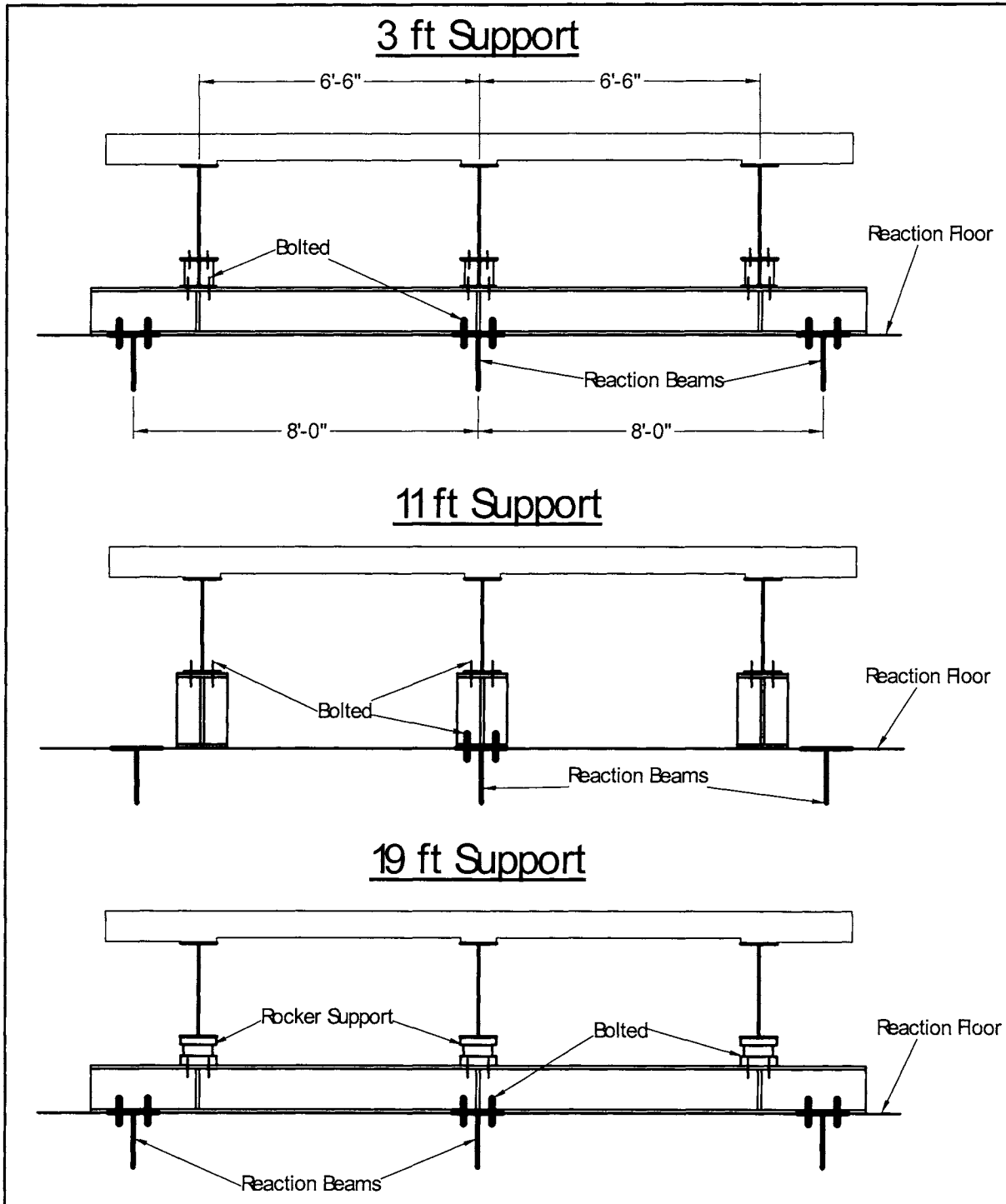


Figure 3. Beam supports.

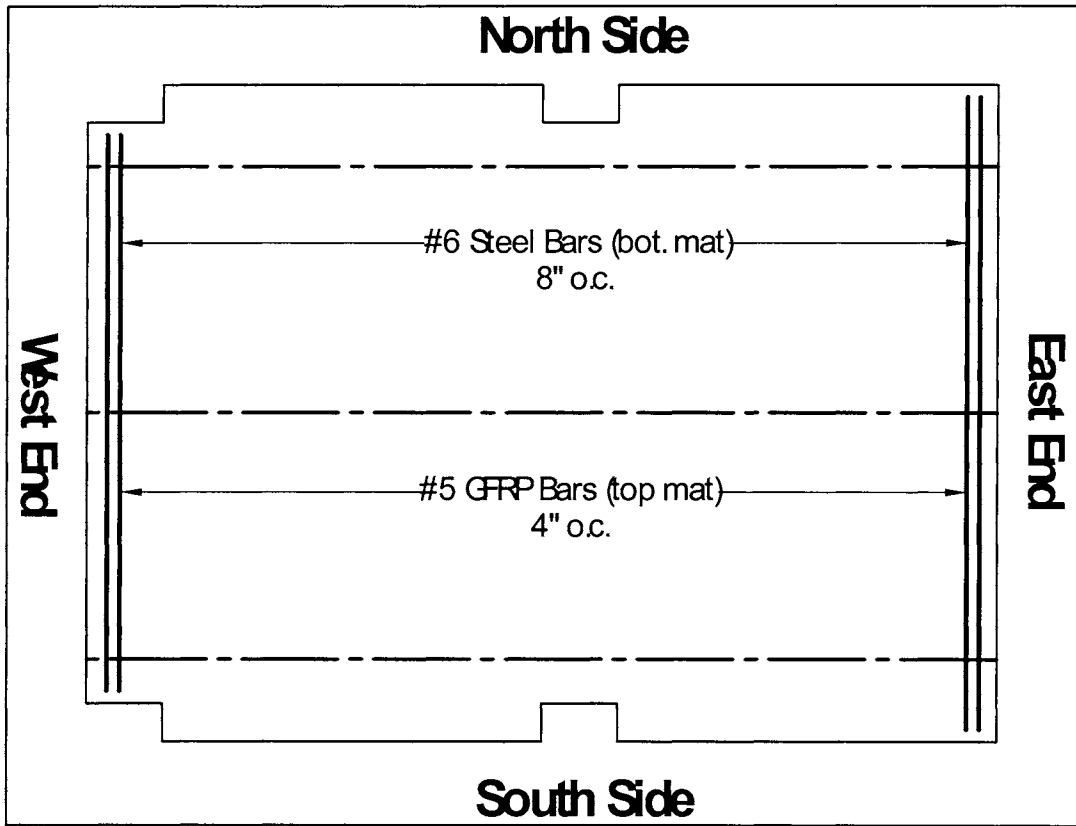


Figure 4. Layout of transverse reinforcing bars.

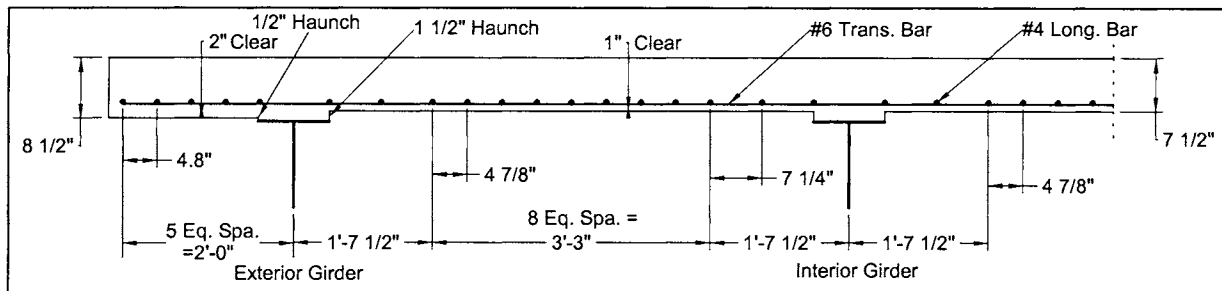


Figure 5. Cross section showing bottom mat bar spacing.

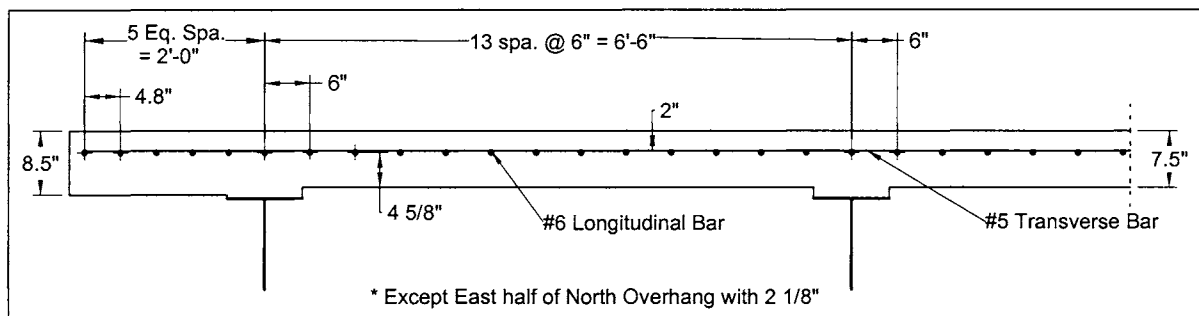


Figure 6. Cross section showing top mat bar spacing.

in by using shorter chairs, but the bars pulled the chairs up off the form work, resulting in a cover depth of only $2\frac{1}{8}$ in. The No. 6 longitudinal bars were spaced at 6 in on center between the interior and exterior girders. From the centerline of the exterior girder to 2 in from the edge of the overhang, there were five equal spaces, and the bars were spaced at approximately $4\frac{4}{5}$ in on center, as shown in Figure 6.

Bridge Deck Construction

Formwork

The girders, with their shear studs previously welded on, were positioned using overhead cranes. Strippable timber formwork was used to form the deck. It was positioned in such a manner that a $\frac{1}{2}$ -in haunch was obtained at the overhangs and a $1\frac{1}{2}$ -in haunch was created between girders. This made the overhangs $8\frac{1}{2}$ in deep and the slab between girders $7\frac{1}{2}$ in deep. The plywood forms were supported on the floor by wood shoring towers (Figure 7).

Steel Reinforcing Bars

One-inch steel bar chairs were laid parallel with the girders between the girders, and 2-in chairs were used on the overhang. The transverse steel was laid down and tied to the chairs. The longitudinal steel was then laid on top of and tied to the transverse steel, as shown in Figure 8.

GFRP Reinforcing Bars

The GFRP reinforcing bars require a special chair and tie wire in order to prevent them from being damaged during construction. The chairs used for this project were plastic chairs, and the tie wire was epoxy-coated steel (Figure 9). On the interior slabs, $\frac{3}{4}$ -in chairs were used; on the south and west half of the north overhang, $5\frac{1}{4}$ -in chairs were used; and on the east half of the north overhang, $4\frac{3}{4}$ -in chairs were used.

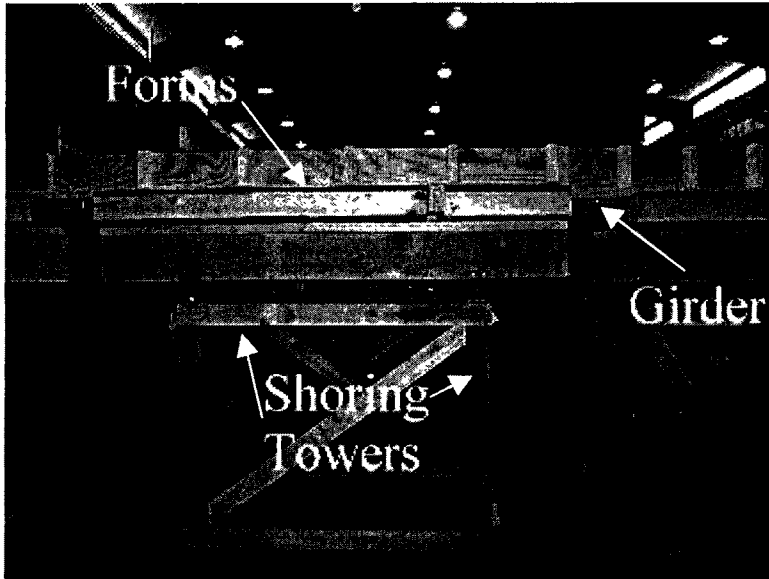


Figure 7. Formwork shoring towers.

Some of the longitudinal bars were placed on the chairs. They were tied to the chairs, and the chairs were then tied to the bottom mat of steel (Figure 9). This was done to keep the GFRP bars from floating because the density of the concrete is greater than the density of the GFRP bars. The transverse bars were then positioned and tied to the longitudinal bars. The

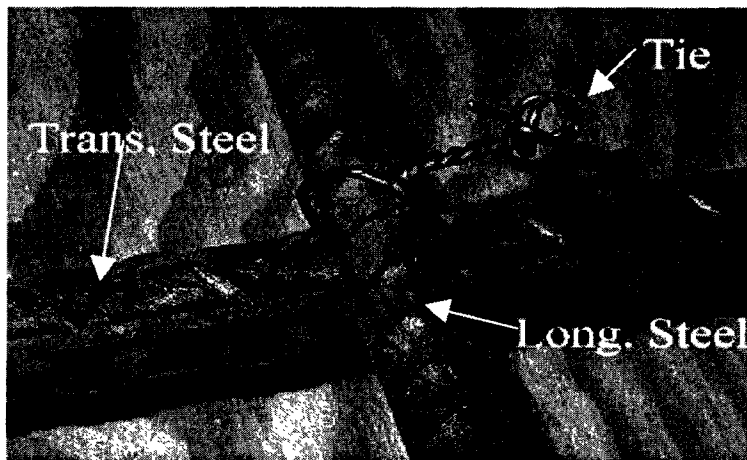


Figure 8. Bottom steel mat tie.

remaining longitudinal bars were then positioned and tied to the transverse bars. The bars supported on chairs were spaced between 2½ ft and 3 ft on center between the girders and 1 ft on center over the girders. The bars were very flexible to stand on at first. As more bars were tied together, the mat became more inflexible. When all bars were tied at each bar intersection, the mat was quite stiff, with the ability to hold a 250-lb man with very little detectable deflection.

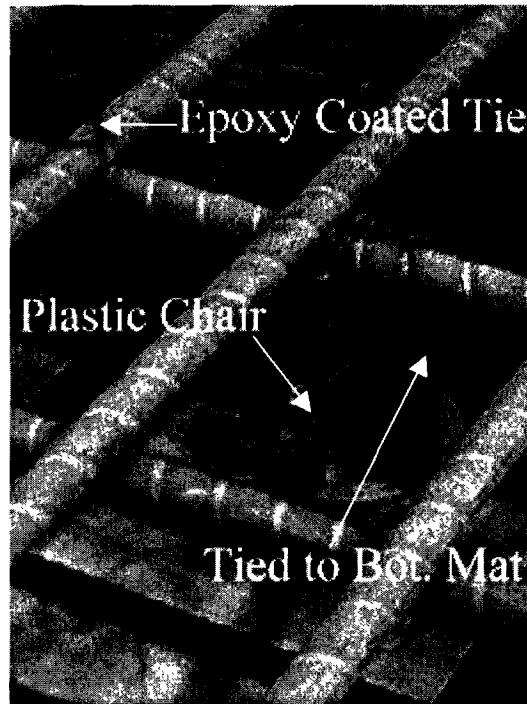


Figure 9. GFRP bar chair.

Placing the Concrete

The concrete was placed using a ¾ cubic yard bucket. The concrete was vibrated as it was placed to ensure proper consolidation. A screed rail was placed along the width of the deck at approximately 12 ft from the east end so that the deck could be placed using two separate concrete batches. The total amount of concrete used was approximately 11 cubic yards, so two separate trucks with batches of 6 and 5 cubic yards were used. After both pours were complete, the screed rail was removed and the void was filled in with concrete. The surface was then finished and 4-in-diameter cylinders were made for each batch of concrete to measure the strength gain over time.

The deck was covered with plastic sheeting and watered for 7 days to obtain a 7-day moist cure. The cylinders were match cured with the deck. The formwork was stripped after 12 days.

Materials

Concrete

The type of concrete used for the deck was a VDOT A4 mix, which is a standard mix for bridge decks. The A4 mix is a 4000 psi mix with 1-in maximum aggregate size, a water-cement ratio of 0.45, a typical slump of 2 in to 4 in, and an air content of $6.5\% \pm 1.5\%$. Test cylinders were made for both of the batches used in the bridge deck. Batch 1 was placed in the east half of the slab, and batch 2 was placed in the west half of the slab. As shown in Table 2, both batches exceeded their 4000 psi minimum strength and batch 2 had a higher strength than batch 1.

Table 2. Concrete Compressive Strengths

Compressive Cylinder Strengths				
Day	Batch 1		Batch 2	
	f_c (psi)	Average (psi)	f_c (psi)	Average (psi)
7	3064	3060	3482	3570
7	3064		3661	
21	4496	4600	5133	5090
21	4695		5053	
28	5252	5150	5769	5550
28	5053		5332	
34	5133	5010	5849	5730
34	4894		5610	
61	5332	5270	6127	6270
61	5212		6406	

Steel Reinforcing Bars

The steel reinforcing bars had a specified yield strength of 60 ksi. Both the No. 4 and No. 6 bars were tested according to ASTM A 370-97a, *Standard Test Methods and Definitions for Mechanical Testing of Steel Products* (1998), in a SATEC Universal Testing Machine (UTM). A clip-on extensometer with a 2-in gauge length was used to measure the strain in the bar, and the computer recorded the applied load. Stress-strain curves were produced for each test. Figure 10 presents a typical curve, from which a modulus of elasticity, E , and a yield strength, f_y , were acquired. The average modulus of elasticity for the bars was 29,100 ksi, and the average yield strength was 70.6 ksi. All modulus and strength data are presented in Tables 3 and 4.

Table 3. Modulus of Elasticity of Steel Reinforcing bars

Bar Size	Test Number	Modulus of Elasticity (ksi)	Average E (ksi)
No. 4	424	28,800	28,400
	425	28,000	
No. 6	426	28,900	29,800
	428	30,600	
Average (ksi)			29,100
Standard Deviation (ksi)			1094
COV (%)			3.76
Low (ksi)			28,000
High (ksi)			30,600

Table 4. Yield Strength of Steel Reinforcing bars

Bar Size	Test Number	Yield strength (psi)	Average f_y (ksi)
No. 4	424	72,700	72.0
	425	71,300	
No. 6	426	69,100	69.2
	428	69,300	
Average (ksi)			70.6
Standard Deviation (ksi)			1.7
COV (%)			2.43
Low (ksi)			69.1
High (ksi)			72.7

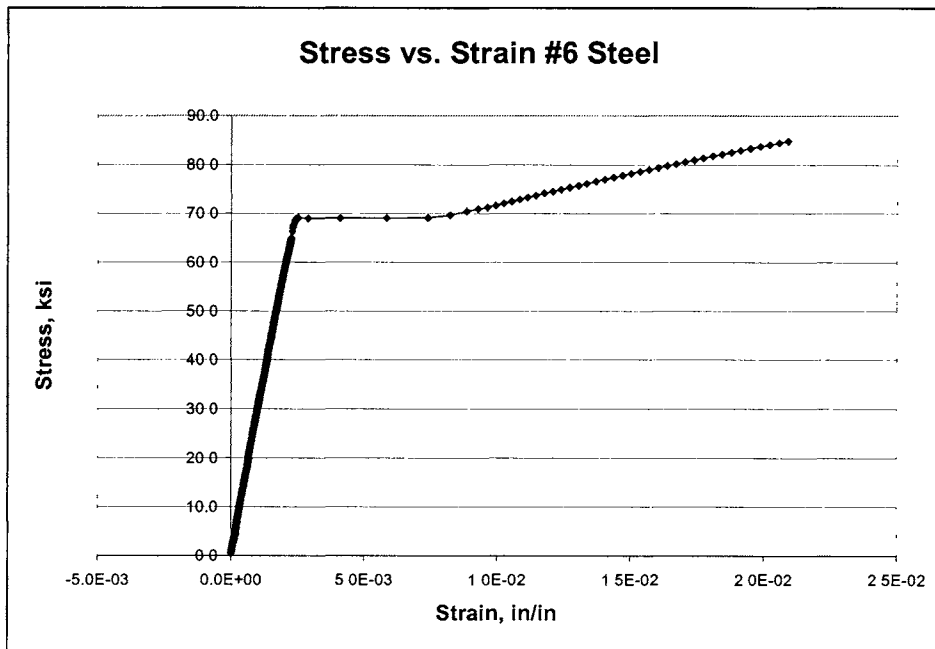


Figure 10. Typical stress-strain behavior of steel reinforcing bars.

GFRP Reinforcing Bars

The GFRP bars used were manufactured by Hughes Brothers, Inc. and are helically wrapped with a mild sand impregnation, as shown in Figure 11. The bars are 73% fiber and 27% resin by volume. The fiber type is E-glass, and the resin type is vinyl ester. The bars were tested in the SATEC UTM using the same procedures and standards as used by DeFreese (2001). A clip-on extensometer with a 2 in gauge length was also used for this test to record the strains, and the computer recorded the applied loads. Stress-strain curves were produced using the data. The stress-strain curves are linear-elastic up to failure; however, the extensometer was taken off before failure to prevent damage.

The No. 5 bars exhibited a linear stress-strain behavior as shown in Figure 12, and the modulus of elasticity was calculated using a best fit line. The stress-strain curve for the No. 6 bars, however, exhibited sudden jumps due to extensometer slip or local fiber failure at the extensometer location, as illustrated in Figure 13. Therefore, the modulus was calculated for each of the straight line portions of each graph and then averaged to obtain a modulus for that particular test. As shown in Table 5, the average tensile strength was 106 ksi for the No. 5 bars and 89.3 ksi for the No. 6 bars. From Table 6 it can be seen that the average modulus of elasticity for the bars was 6,210 ksi. During analysis of the deck, a modulus of 6,300 ksi was used based on earlier work by DeFreese (2001). DeFreese (2001) tested three different sizes of Hughes Brothers bars and tested five samples of each bar size. Three different types of instrumentation measured the strain in the bars: strain gauges, an extensometer with a 2 in gauge length, and linear variable differential transformers (LVDTs) with a 7.5 in gauge length.



Figure 11. Hughes Brothers GFRP bar.

Table 5. GFRP Bars Ultimate Tensile Strength

Bar Size	Measured Tensile Strength, psi					Average ksi	COV %
	Test 435	Test 436	Test 437	Test 438	Test 439		
No. 5	100,960	110,864	104,288	99,658	115,298	106	6.29
No. 6	92,823	93,406	*	87,007	84,033	89.3	5.10

* test accidentally aborted before failure.

Table 6. GFRP Bar Modulus

Bar Size	Test #	Modulus of Elasticity, ksi	Average, ksi
No. 5	435	6013	6120
	436	6320	
	437	6034	
	438	6146	
	439	6102	
No. 6	429	6461	6300
	430	6388	
	431	6145	
	433	6309	
	434	6208	
Average, ksi			6210
Standard Deviation, ksi			151
COV			2.44
Low, ksi			6013
High, ksi			6461

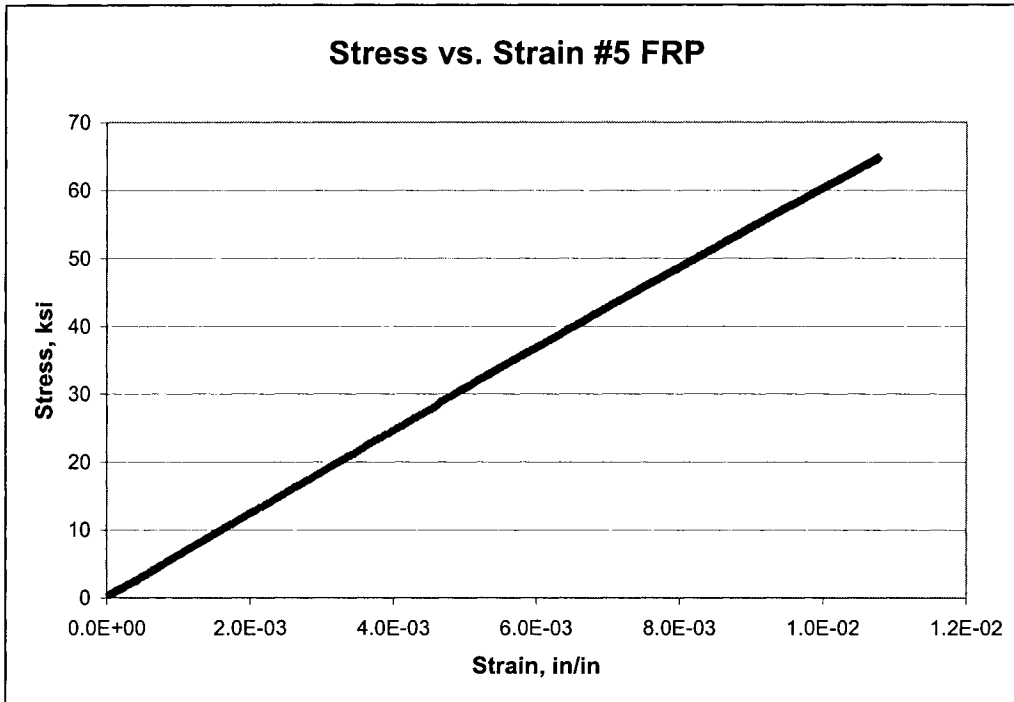


Figure 12. Typical stress-strain plot for No. 5 GFRP bars.

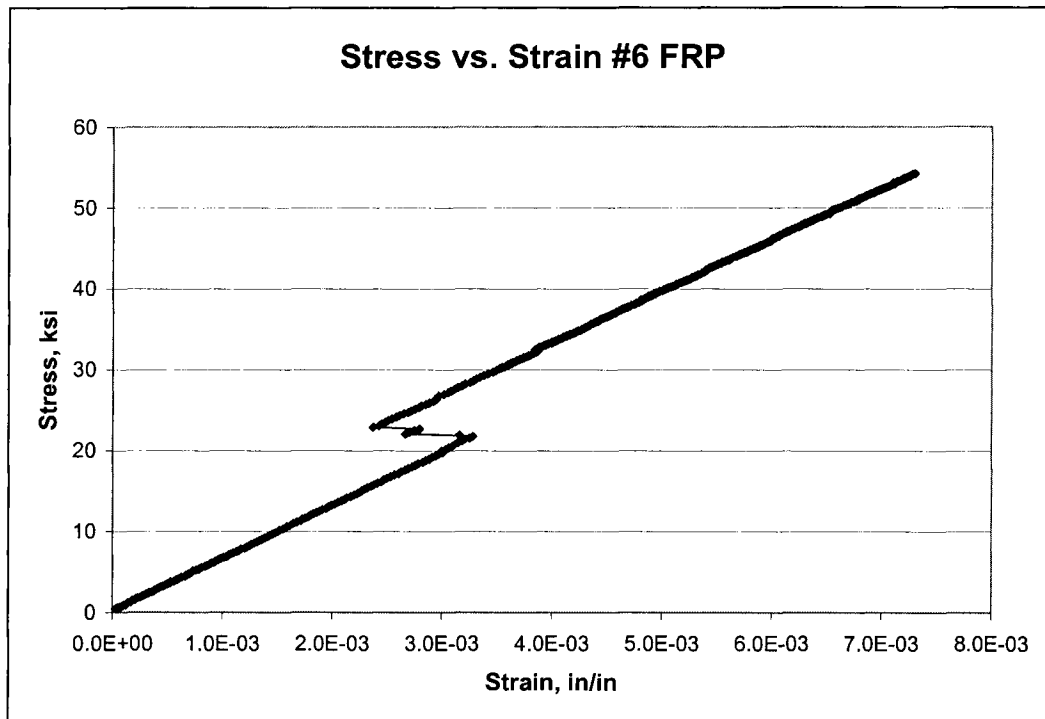


Figure 13. Typical stress-strain behavior for No. 6 GFRP bars.

Instrumentation and Test Setup

Overhang Tests 1 and 2

Overhang Tests 1 and 2 were designed to simulate a typical AASHTO design truck tire on the edge of the overhang, which would create a negative moment in the deck over the exterior girder. This load is harsher than reality because the bridge will have a barrier rail on the overhang that will prevent a wheel load from being applied to the overhang. The instrumentation and test setup for Overhang Tests 1 (south side) and 2 (north side) were similar. The only differences between the two were in strain gauge locations. These differences were no more than ½ in and were due to slight variations in bar placement.

Instrumentation

Each of the two overhang tests had eight No. 5 transverse GFRP bars strain gauged and four No. 6 transverse steel bars strain gauged. Both the GFRP and steel strain gauges were positioned on the bars above the outer edge of the exterior girder's flange. This distance measured 21 in from the edge of the overhang. For Overhang Test 1, south side, and for Overhang Test 2, north side, the gauges were positioned as shown in Figure 14. The steel gauges, also on transverse bars, were positioned as shown in Figure 15. All of the strain gauges for all of the tests were oriented along the length of the particular bar to which they were affixed.

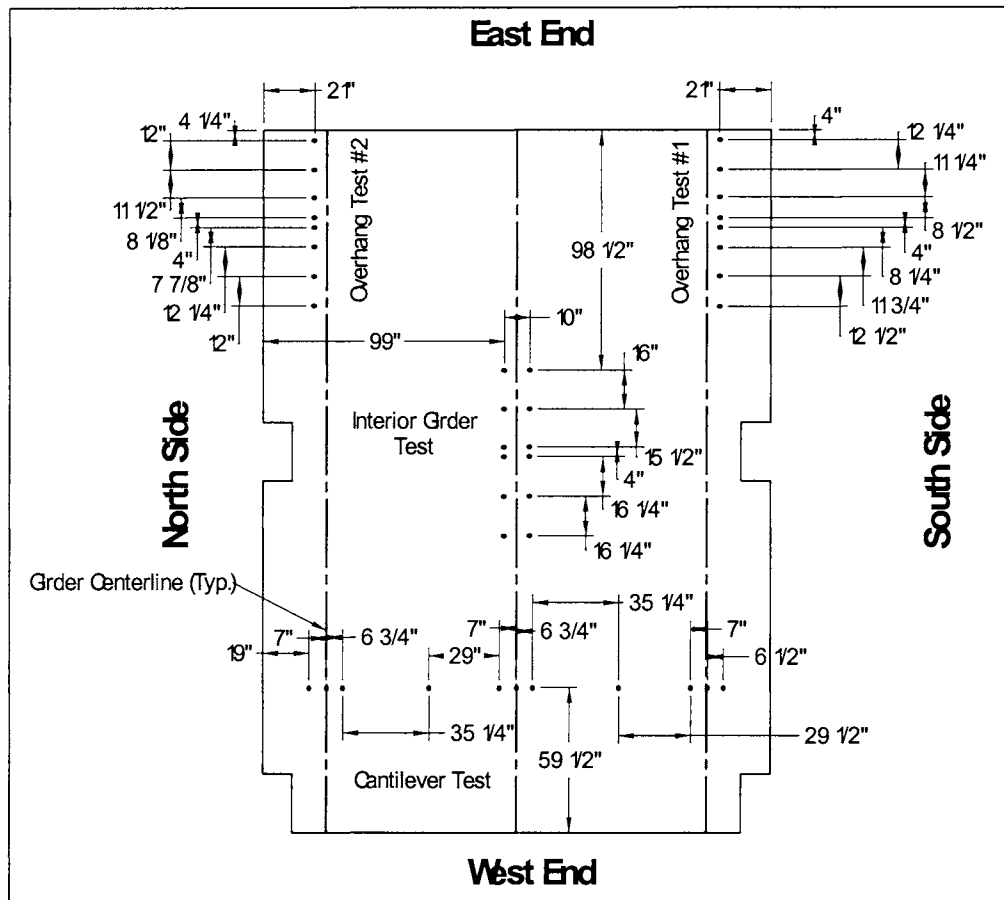


Figure 14. Strain gauges on top mat reinforcement.

The wire pots used to measure deflections were in similar locations for both overhang tests. They were anchored to the bottom of the slab at $\frac{1}{2}$ in from the edge. The first pot was located 8 in from the east end of the slab, and the other five were positioned 12 in on center from the first, as shown in Figure 16.

Whittemore gauge points were placed 4 in on either side of the outer edge of the exterior girder for a total gauge length of 8 in. Overhang Test 1 had eight points, and Test 2 had seven points. The first set of gauges was located 8 in from the east edge of the slab (Figure 17), and all others were 12 in on center from the first.

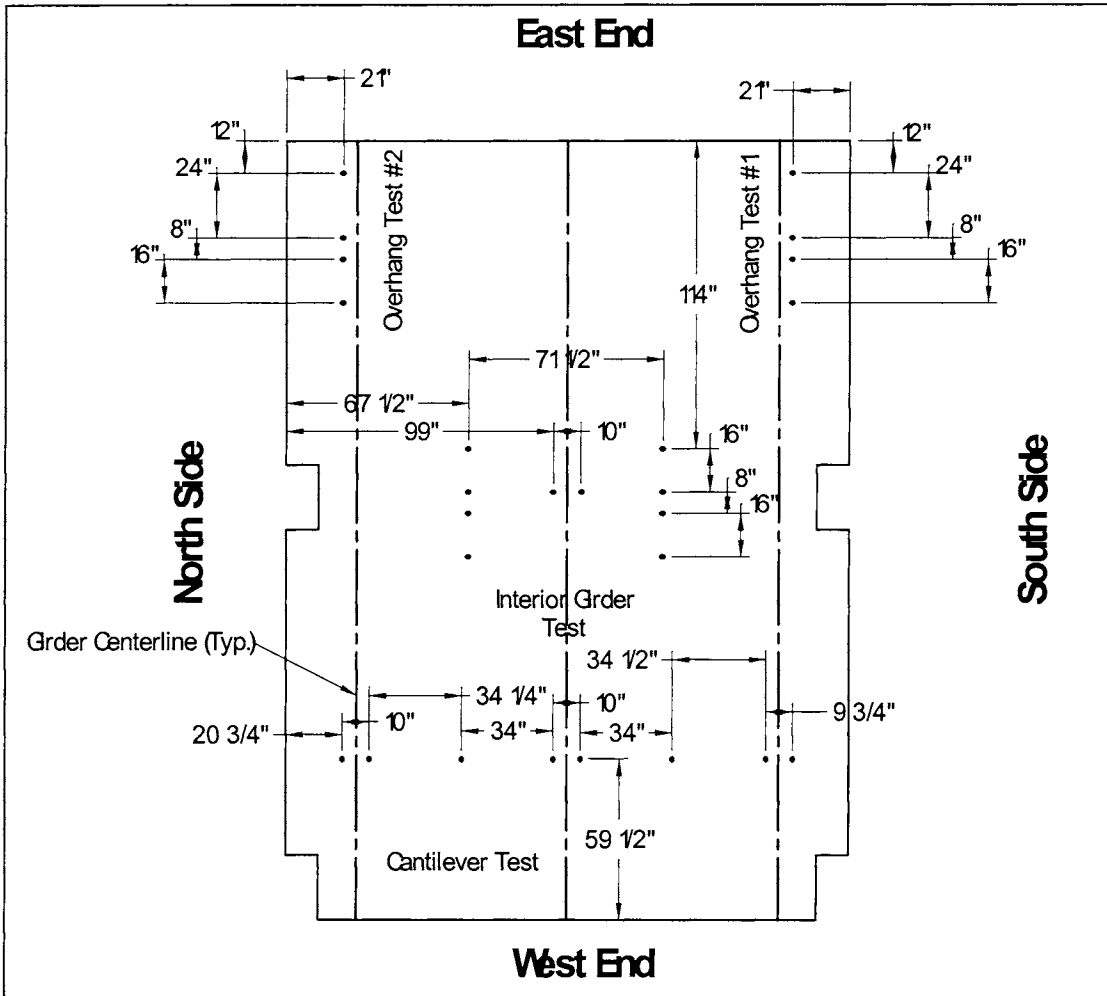


Figure 15. Strain gages on bottom mat reinforcement.

Test Setup

The load frame ran parallel with the bridge girders, with one column placed in the notched out section and the other column placed at the east end of the deck. The columns for the load frame were bolted to the reaction floor beam, and a cross beam was bolted to their flanges. The cross beam had a moment end plate on both ends and a stiffener located at the load point. A 120-kip capacity hydraulic load ram was suspended from the cross beam with a 200-kip capacity load cell placed between the ram and cross beam to measure the loads.

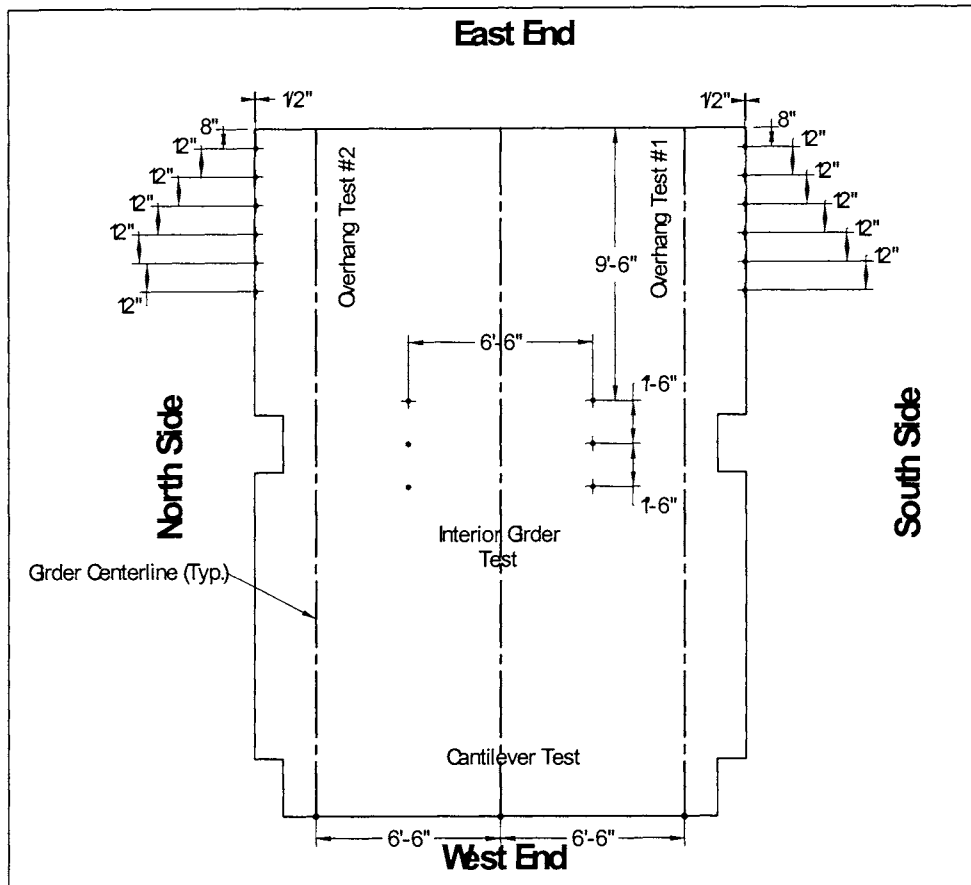


Figure 16. Wire pot locations.

The load was applied to the overhang by an 8 in by 20 in patch load to resemble a truck tire patch. These patch dimensions were calculated using Equation 1, as presented in AASHTO (1998).

$$Tire\ Width = \frac{P}{0.8} \quad (1)$$

$$Tire\ Length = 6.4 \cdot \gamma \cdot \left(1 + \frac{IM}{100}\right)$$

Where : P = wheel load, kips

γ = load factor

IM = impact factor, percent

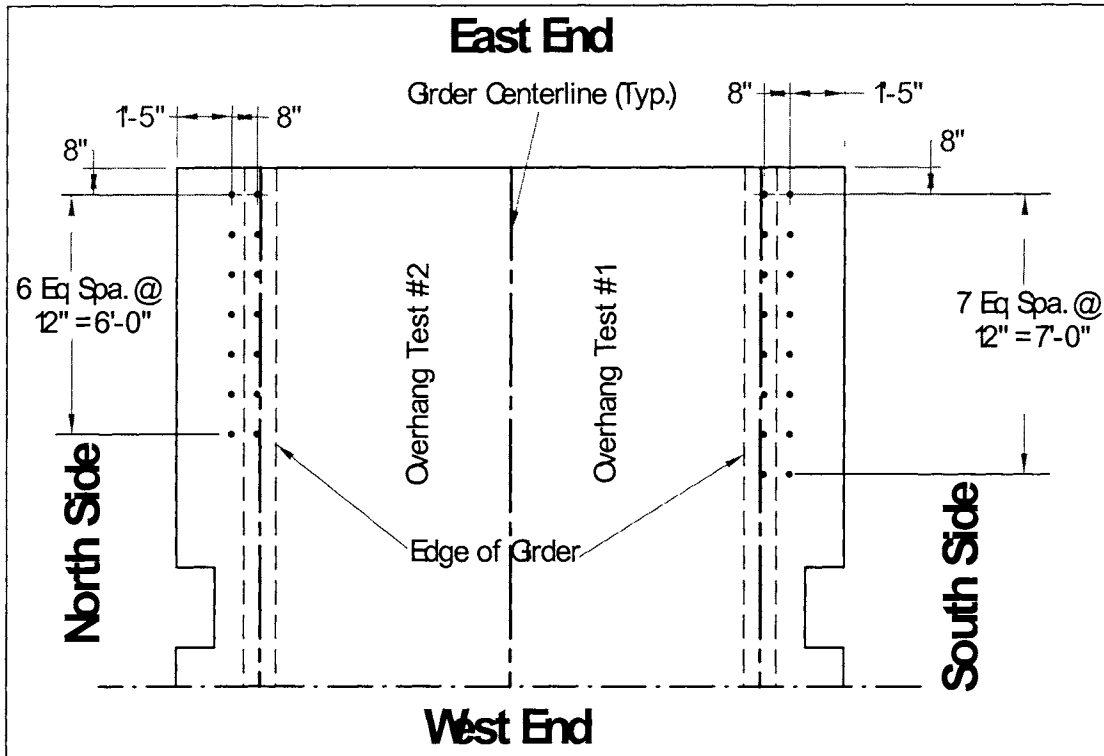


Figure 17. Whittemore gauge locations.

With a wheel load of 16 kips, a load factor of 1.0, and an impact factor of 30%, the width and length were calculated to be 20 in and 8.3 in, respectively. A patch load of 20 in by 8 in was selected to match available plates and pads. A neoprene pad was placed directly on the concrete, and a modified steel plate was placed on top of the pad as shown in Figure 18. The ram applied load to the plate, which was stiff enough to distribute the load uniformly to the pad. The center of the patch load was positioned 3 ft 2 in from the east end, and the edge of the pad and steel plate were flush with the edge of the deck (Figure 19).

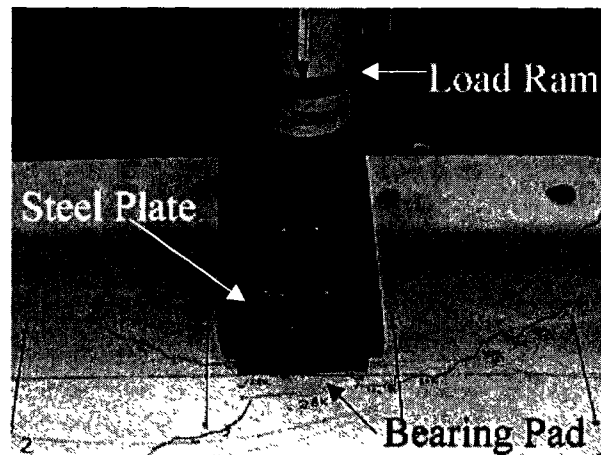


Figure 18. Wheel patch load.

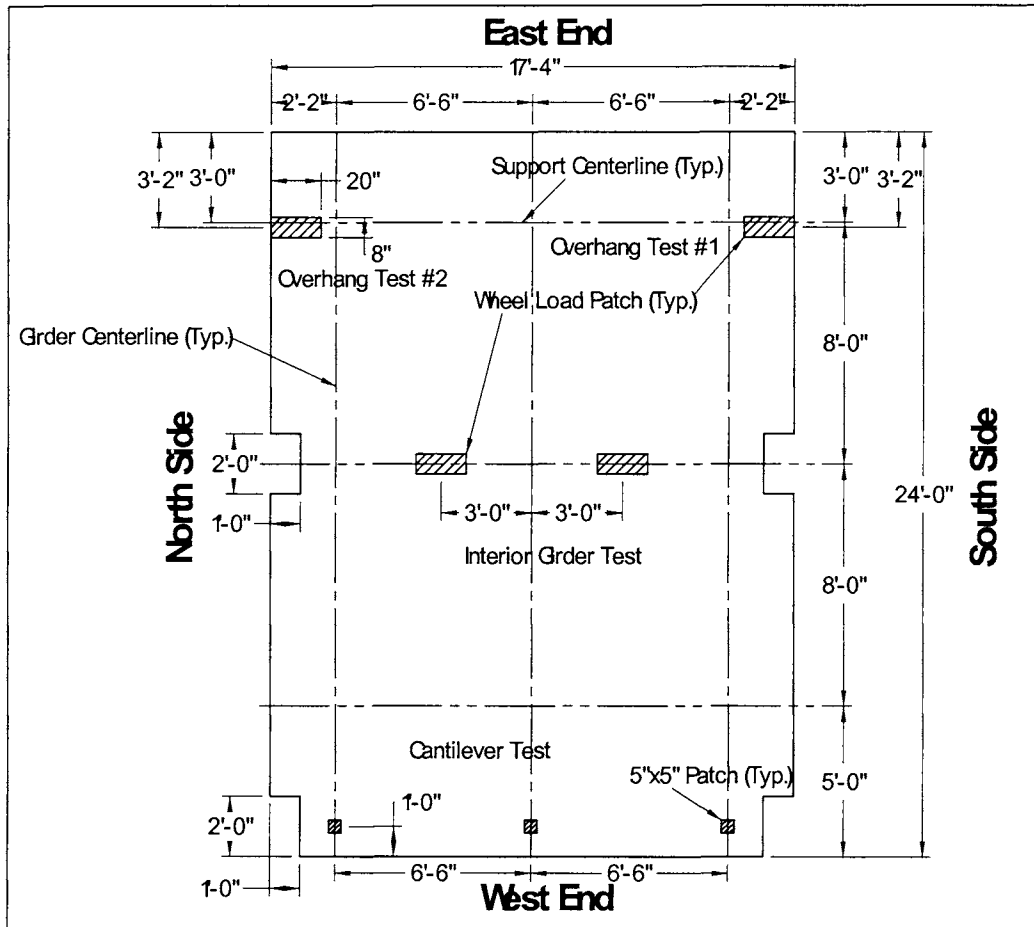


Figure 19. Positions of load application.

Interior Girder Test

The interior girder test was performed to simulate a typical AASHTO design truck traveling over the center of an interior girder with its axle perfectly straddling the girder. This creates a maximum negative moment over the interior girder.

Instrumentation

This test used 10 strain gauges on steel reinforcing bars and 12 gauges on GFRP bars, all of which were located on transverse bars. Six GFRP bars were gauged, with 2 gauges on each bar. The gauges were 10 in apart and positioned so that the gauges were above either edge of the interior girder's top flange. The gauges were positioned to straddle the middle support with three equally spaced rows on either side. The rows of 2 gauges were located as shown in Figure 14.

Two of the steel strain gauges were positioned similarly to the GFRP gauges in that they were placed above either edge of the interior girder's top flange. The remaining 8 were on 4 bars, 2 per bar. The gauges were positioned under the load points to measure stresses at the location of maximum positive moment. The pairs were positioned as shown in Figure 15.

Wire pots used to measure deflections were symmetrically placed on each side of the interior girder. They were anchored to the bottom of the slab at 3 ft 3 in from the centerline of the interior girder on either side. The locations of the wire pots are shown in Figure 16.

Test Setup

The two columns for the load frame were placed in the notched out sections of the slab 11 ft from the east end. The columns were bolted to the reaction floor beams, and the cross beams were bolted to the columns. A 400-kip capacity hydraulic ram and a 500-kip capacity load cell were suspended from the crossbeams directly over the interior girder. The load was applied to the slab through two 8 in by 20 in neoprene pads with steel plates placed on top of them. The centers of the pads were placed 3 ft to either side of the centerline of the interior girder and 11 ft from the east end. A spreader beam was placed on top of both load plates running along the width of the slab. The ram applied load to the center of the spreader beam, which transferred equal load to the two patches (Figure 19).

Cantilever Test

The cantilever test was performed to simulate negative moments over interior supports in continuous span structures. Although the actual design comprises simple spans, this test was performed to examine the behavior of GFRP-reinforced decks in continuous bridges.

Instrumentation

This test used 11 strain gauges on GFRP bars, 8 strain gauges on steel reinforcing bars, and 6 strain gauges on the webs of the girders. Of the 11 GFRP strain gauges, 3 were positioned on longitudinal bars over the centers of each girder, 6 were positioned on longitudinal bars on either edge of the top flange of each girder, and the other 2 were positioned on longitudinal bars halfway between the three girders. They were positioned as shown in Figure 14. All were positioned 59½ in from the west edge of the slab.

Of the 8 steel reinforcing bar strain gauges, 6 were positioned on longitudinal bars on either edge of the top flange of each girder, and the other 2 were positioned on longitudinal bars halfway between the three girders. They were positioned as shown in Figure 15. All were located 59½ in from the west edge of the slab. All of the 6 steel strain gauges on the webs of the three girders were located approximately 58 in from the west end of the girders. On each girder, 1 gauge was located approximately $3\frac{7}{16}$ in from the bottom of the girder, and 1 was located approximately $3\frac{7}{16}$ in from the top of the girder.

One wire pot was attached to the bottom of each girder with a magnet. The pots were positioned at the west end of each of the girders (Figure 16).

Test Setup

The two columns for the load frame were placed in the notched out sections of the slab at the west end. The columns were bolted to the reaction floor beams, and the cross beams were

bolted to the columns. Three 400-kip capacity hydraulic rams were used for this test. One was positioned over each of the girders. The two rams over the exterior girders were hung with 200 kip capacity load cells, and the ram over the interior girder was hung with a 500-kip capacity load cell. Load was applied to the slab through 5 in by 5 in neoprene pads with steel plates on top of them. Wheel patch pads were not used, because this test was not investigating local effects, but total negative moment over the support. The pads were located over the top of each girder, and they were all 1 ft from the West end (Figure 19).

Test Procedures

All of the instrumentation devices, the strain gauges, wire pots, and load cells, were connected to a System 6000 data acquisition system. The Strain Smart software program was used to record the data. All the channels of the data acquisition system were zeroed, and an online display of all the channels and their readings was created so the data could be monitored during testing.

Overhang Tests 1 and 2

A preload of 5 kips was applied to the overhangs to allow the structure to settle, and the overhangs were then unloaded. Load was applied to the overhangs in 2-kip increments, and data were recorded at each increment. This was continued until it was determined that the section was cracked, 30 kips for Test 1 and 32 kips for Test 2. The overhangs were then unloaded and reloaded up to a service wheel load times an impact factor, 21 kips. This was done three times to examine changes in stresses, crack widths, and deflections at service loads after cracking.

Each overhang was loaded again from the previous load in 2-kip increments until a total load of approximately 40 kips was on the overhang. At this point, the load increments were increased to 4 kips up to failure, and data were recorded at each increment.

Throughout the entire process, the overhang was continuously checked for cracks and the crack widths were measured using crack cards. Whittemore gauge readings were also taken at various loads throughout the testing.

Interior Girder Test

A preload of 10 kips was applied to the spreader beam, 5 kips per patch load, to allow the structure to settle, and then the deck was unloaded. The load was applied to the spreader beam in 10-kip increments up to a load of 160 kips, and data were recorded at each increment. The increments were then increased to 20 kips up to failure.

The deck was continuously checked for cracks throughout the test. Once cracking occurred, selected cracks were labeled and their widths were measured at various loads using a crack microscope. The crack microscope was used to provide greater accuracy than could be achieved with the crack comparator cards.

Cantilever Test

The two exterior hydraulic rams for this test were connected in series, and the interior ram was connected separately. The loads were kept approximately equal on each ram by using the online display of the loads as measure by the load cells.

A preload of 10 kips was applied to each ram to allow the structure to settle, and then the bridge was unloaded. Load was applied to the cantilever through each ram in 10-kip increments and data were recorded at each increment. This was continued until it was determined that the section was significantly cracked, 110 kips on each ram. The cantilever was then unloaded to 10 kips and loaded up to a service load, about 80 kips. This was done 5 times to examine any changes in behavior through several cycles of expected service load moment. The load was taken back up to 110 kips and continued in 10-kip increments until a load of 140 kips was reached. The section was not loaded to failure due to inadequate capacity of the load cells and load frames.

The deck was continuously checked for cracks throughout the test. Once cracking occurred, selected cracks were labeled and their widths were measured at selected load increments, including the service cycling, using a crack microscope.

RESULTS AND DISCUSSION

Overhang Tests 1 and 2

Introduction

During the tests of the bridge deck overhangs, measurements were taken to obtain deflection information, GFRP reinforcing bar stresses, cracking loads, crack widths, and failure load and mode. The following sections present the results of these two tests and compare measured behavior to behavior predicted using relatively simple analytical approaches.

Deflections

Overhang Test 1

For both overhangs, the deflections were measured using wire pots that were anchored to the bottom of the deck. The collected data were used to create load vs. deflection plots for each wire pot. Figure 20 presents the load vs. deflection data for two wire pots on Overhang Test 1. The graph also contains deflections predicted using two theoretical models based on current design guides and equations.

The deflections labeled “Theoretical” were calculated using the more basic of the two theoretical models. The effective width of the overhang was calculated using Equation 2 as presented in Table 4.6.2.1.3-1 of *AASHTO LRFD Bridge Design Specifications* (1998) and shown here:

$$EW_{\text{overhang}} = 45\text{in} + 0.833X \quad (2)$$

Where : EW_{overhang} = effective width of overhang, in

X = distance from load to point of support, in

The effective width was calculated to be 4½ ft using an X of 11 in. The deck was modeled as a 12-in-wide strip in the analysis program RISA-2D (RISA Technologies 1993) with the girders modeled as pin supports. For the exterior girder closest to the overhang test, the

exterior edge of the girder was modeled as a pin support. The load was applied to the beam at a distance of 11 in from the exterior edge of the girder. The loads applied in the analysis were the applied test loads divided by the effective width of the overhang, to obtain an “effective load” on the 12-in-wide section.

Transformed moments of inertia, I_t , of 443.4 in⁴ and 629.9 in⁴ were used for the interior slab (7.5 in thick) and overhang portions (8.5 in thick), respectively. Sample calculations of cross-sectional properties are provided in Appendix B. Once the estimated cracking load of 26 kips, 5.78 kips effective load, was reached, a cracked moment of inertia, I_{cr} , of 47.9 in⁴ was used to model the overhang portion of the slab. The loads and their corresponding deflections were calculated and plotted.

The deflections labeled “Theo. I_{eff} ” were calculated in a fashion similar to “Theoretical” except an effective moment of inertia, I_e , was used for the overhang portion of the slab after cracking. Equations 3 and 4, as presented in ACI 440 (ACI 2001) and shown here, were used to calculate the effective moment of inertia.

$$I_e = \left(\frac{M_{cr}}{M_a} \right)^3 \beta_d I_g + \left[1 - \left(\frac{M_{cr}}{M_a} \right)^3 \right] I_{cr} \leq I_g \quad (3)$$

Where : I_e = effective moment of inertia, in⁴

M_{cr} = cracking moment, in - k

M_a = max moment in a member at particular load, in - k

I_g = gross moment of inertia, in⁴

β_d = reduction coefficient

I_{cr} = cracked moment of inertia, in⁴

$$\beta_d = \alpha_b \left[\frac{E_f}{E_s} + 1 \right] \quad (4)$$

Where : α_b = bond dependent coefficient, 0.5

E_s = modulus of elasticity of steel, 29,000 ksi

E_f = modulus of elasticity of FRP, 6,300 ksi

Equation 3 is valid only for values of $M_a > M_{cr}$. In Equation 3, the transformed moment of inertia, I_t , was used in place of the gross moment of inertia, I_g . The difference between the two is very small, but the use of the transformed moment of inertia should yield more accurate results.

M_a was calculated by multiplying the effective load by 11 in, the distance from the load point to the edge of the girder. Equation 5 was used to calculate the cracking moment M_{cr} .

$$M_{cr} = \frac{f_t I_t}{y} \quad (5)$$

Where : I_t = transformed moment of inertia, in⁴

M_{cr} = cracking moment, in - lb

$f_t = 7.5\sqrt{f_c'}$, concrete tensile strength, psi

f_c' = concrete compressive strength, psi

y = distance to centroid from surface, in

For the RISA-2D (RISA 1993) analysis, I_e was equal to I_t up to a load of 32.1 kips. At this load, the effective load was calculated to be 8.02 kips, and M_a was 7.35 ft-kips, which exceeded the value of M_{cr} , 6.47 ft-kips. The value of f_c' used was 5,010 psi. This was the 34 day batch 1 average. Both overhangs were poured with batch 1 and were tested at about 34 days.

As shown in Figure 20, both theoretical approaches predict the measured deflections well up to a load of about 26 kips. The two theoretical approaches predict the same deflections up to a load of 26 kips, because they are both using I_t for the moment of inertia of the overhang. At around 24 kips, there is a slight slope change in the measured load-deflection curve, indicating that the section has become less stiff and non-visible cracking may have occurred. Cracking is assumed to occur in the Theoretical deflection model at a load of 26 kips. At this point I_{cr} is used as opposed to I_t . This causes a noticeable jump in the plot, whereas the measured deflection curve has more of a gradual slope change during cracking. The jump can be attributed to the sudden change from uncracked to cracked properties, however the actual change is more of a gradual process as cracking progresses.

The Theo. I_{eff} approach more accurately models this gradual slope change, but the change occurs at the much higher load of 32 kips, which was determined from the measured deflections. The gradual slope change can be attributed to the fact that I_{eff} is formulated to decrease constantly with increased moment, starting at the predicted cracking moment. Because I_e is constantly decreasing, the slope is constantly decreasing as well. This is a more accurate representation of actual behavior as shown by the experimental data.

A second and more major slope change occurs in the measured deflection curve around a load of 32 kips. This slope change is not seen in the calculated deflections. One contributor to these increased deflections may be shear deflections, which are not accounted for in the theoretical models. Deflections in short spans are known to be dominated by shear, especially at higher loads, as is the case here. Other contributors may include support deflection (at the girder flange), which was not measured; the fact that the east end was a cantilever that was allowed to deflect during the test; and the concrete stress-strain behavior becomes non-linear at higher loads, above approximately 40 kips.

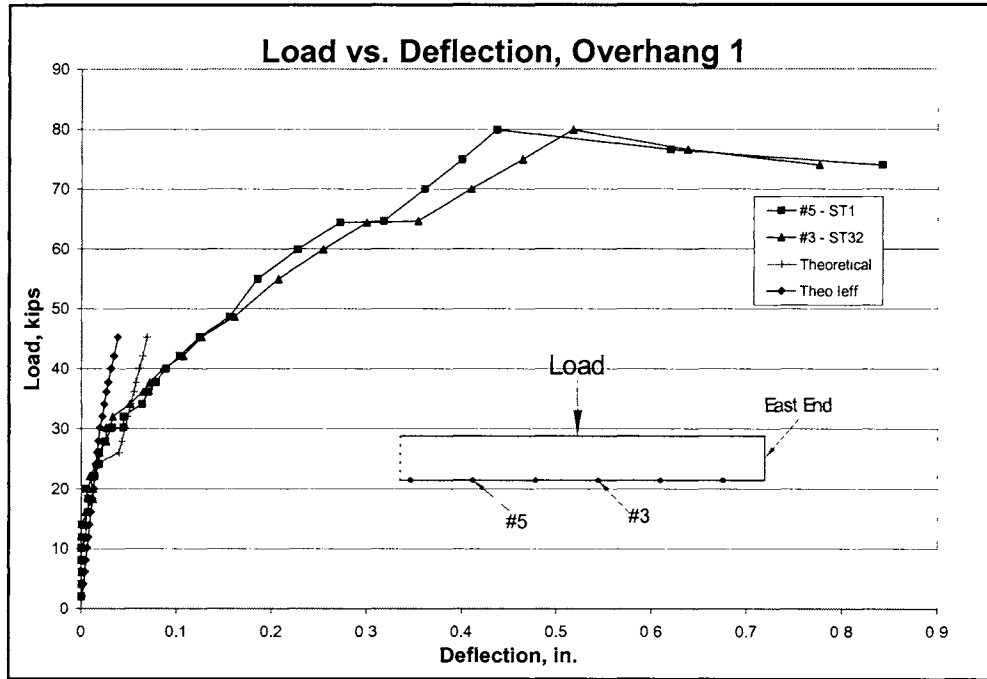


Figure 20. Load-deflection plot for Overhang 1.

Overhang Test 2

Overhang Test 2 was performed, and data were collected in the same manner as for Test 1. Load vs. deflection data are presented in Figure 21. The theoretical deflection calculations were identical with the exception of a few values. I_t for Overhang 2 was 629.6 in^4 , I_{cr} was 46.2 in^4 , but M_{cr} remained 6.47 ft-kips. For the Theoretical deflections, the estimated crack load was lowered to 20 kips, 4.44 kips effective, based on observations and other data. Therefore, at 20 kips, the deflections in the overhang section were calculated using I_{cr} as opposed to I_t . For the Theo. I_{eff} method, I_e was equal to I_t up to a load of 32 kips.

As shown in Figure 21, the theoretical deflections are quite similar to the measured values but only up to a load of about 16 kips. At this point, the slope of the measured load-deflection curve gradually begins to decrease, indicating possible cracking. At about 20 kips, this slope change is a little more obvious and the section is now modeled as fully cracked in the Theoretical deflection curve. Using the fully cracked properties predicts the measured deflections well to approximately 30 kips.

The approach presented as Theo I_{eff} does not accurately predict deflections after cracking because of its high modeled cracking load of 32 kips. It does, however, model the gradual slope change well. As in the Test 1 graph, the measured deflections begin to increase more rapidly at a load of about 32 kips, which is not modeled by the theoretical deflection models. This can again be attributed to shear deflections, support deflections, east end cantilever deflections, and non-linear concrete stress-strain behavior.

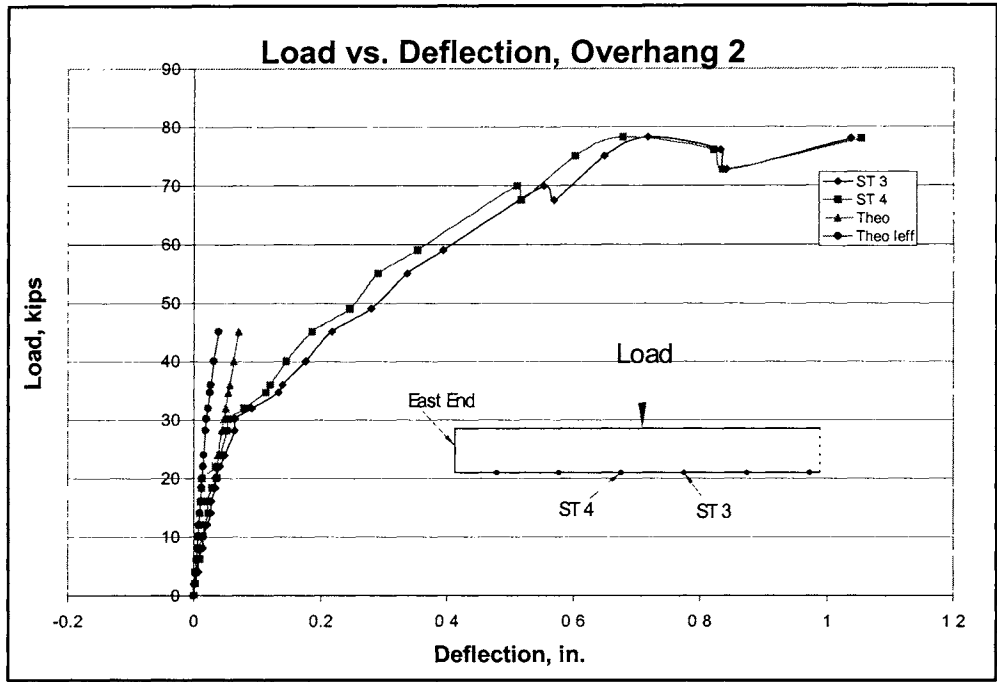


Figure 21. Load-deflection plot for Overhang 2.

Reinforcing Strains and Stresses

Overhang Test 1

The strain gauge data acquired by the System 6000 were reduced, and load vs. strain plots were created for both the steel and GFRP gauges. Figure 22 is a plot of load vs. steel reinforcing bar strains. Steel gauge 1 on the plot has a fairly constant negative slope up to a load of 46 kips, indicating that the bar is below the neutral axis and is in compression. Just past 46 kips, the strain takes a large jump and becomes positive, indicating that the bar is now above the neutral axis and is in tension. The change in neutral axis location is due to cracking in the concrete above the bar. Calculations of I_{cr} indicate that the neutral axis is below the steel after cracking.

Steel gauge 3 follows the same pattern as gauge 1, only the strains are constant and close to 0 up to a load of 24 kips. This would indicate that the bar is fairly close to the neutral axis. At a load of 26 kips, the strains show a large increase into the tension region. This once again indicates that a crack in the concrete has opened and the neutral axis has dropped below the bar, causing it to go into tension. This happens at 26 kips as opposed to 46 kips because gauge 1 is closer to the load and cracking occurred there first.

Figure 23 is a load vs. strain plot for GFRP gauges 30 and 31 which were located 2 in to either side of the load. The plot shows both gauges measuring approximately the same strains, which is expected because they are approximately the same distance away from the load. They both have a relatively constant positive slope up to a load of about 22 kips. This indicates that they were both located above the neutral axis and were in tension. At a load of 24 kips, the slope starts to decrease, indicating that the section has cracked, the neutral axis has been lowered, and therefore strains in the bars are increasing more for the same load increment. The slope

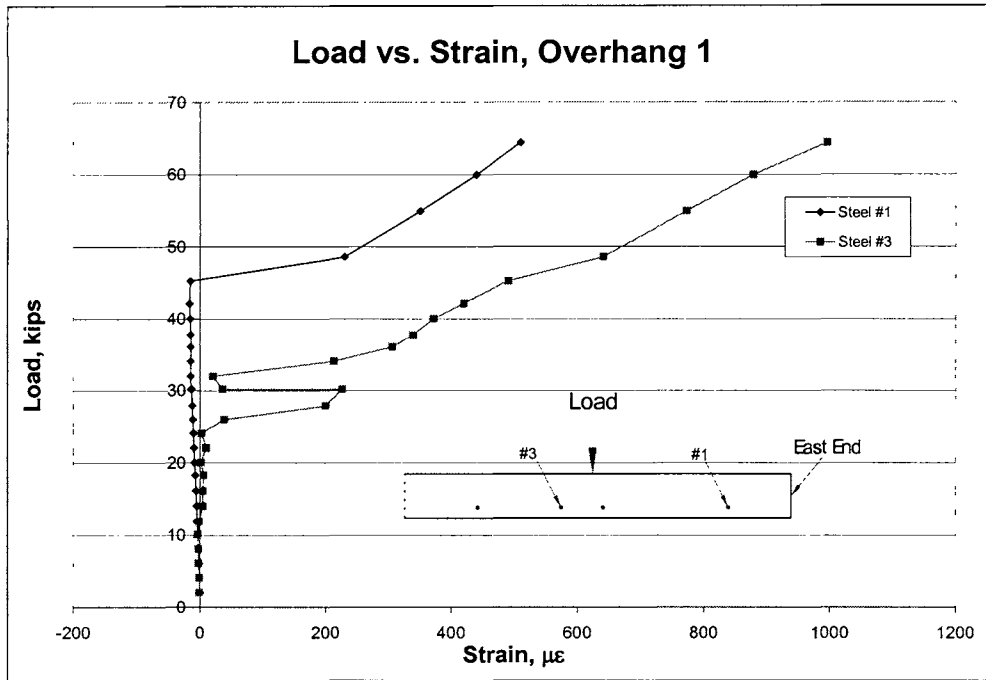


Figure 22. Load vs. strain plot for Overhang 1, steel gauges.

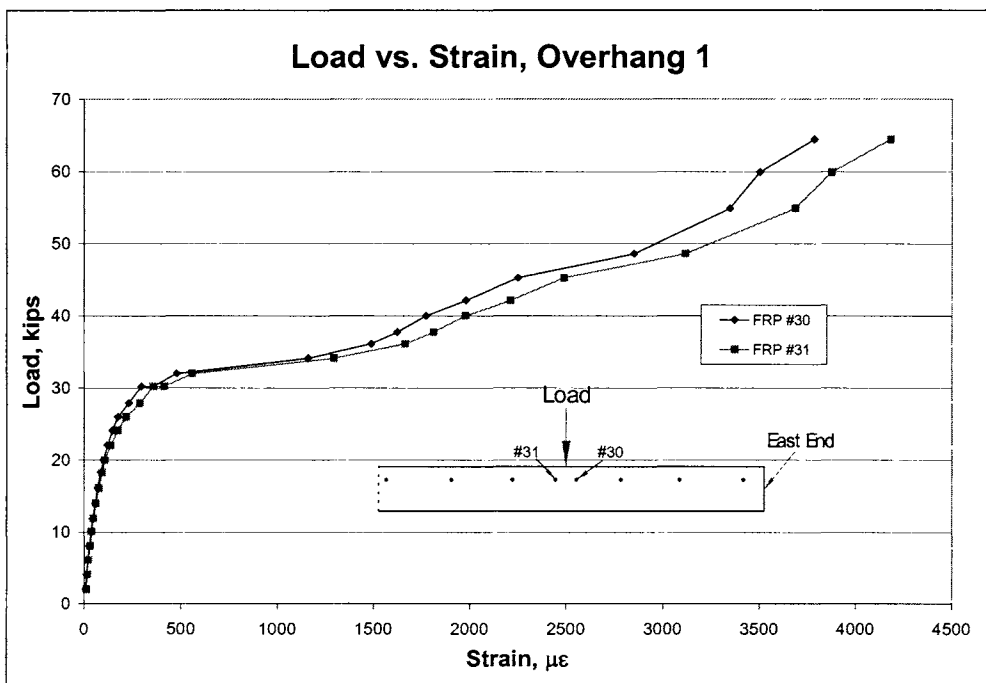


Figure 23. Load vs. strain plot for Overhang 1, GFRP gauges.

continues to decrease up to a load of about 32 kips, where it almost reaches zero slope, and then increases again at 36 kips, at which point it stays relatively constant.

The stresses in the GFRP bars were obtained by multiplying the recorded strains by the modulus of elasticity of the GFRP bars, 6,300 ksi. Stress profile curves were then created at various loads. These plots show the stress in each bar relative to its distance from the load point. Figure 24 is a stress profile plot for loads of 16 kips and 20 kips before cracking. As can be seen and as expected, the stresses are high close to the load and taper off as gauges get further away from the load.

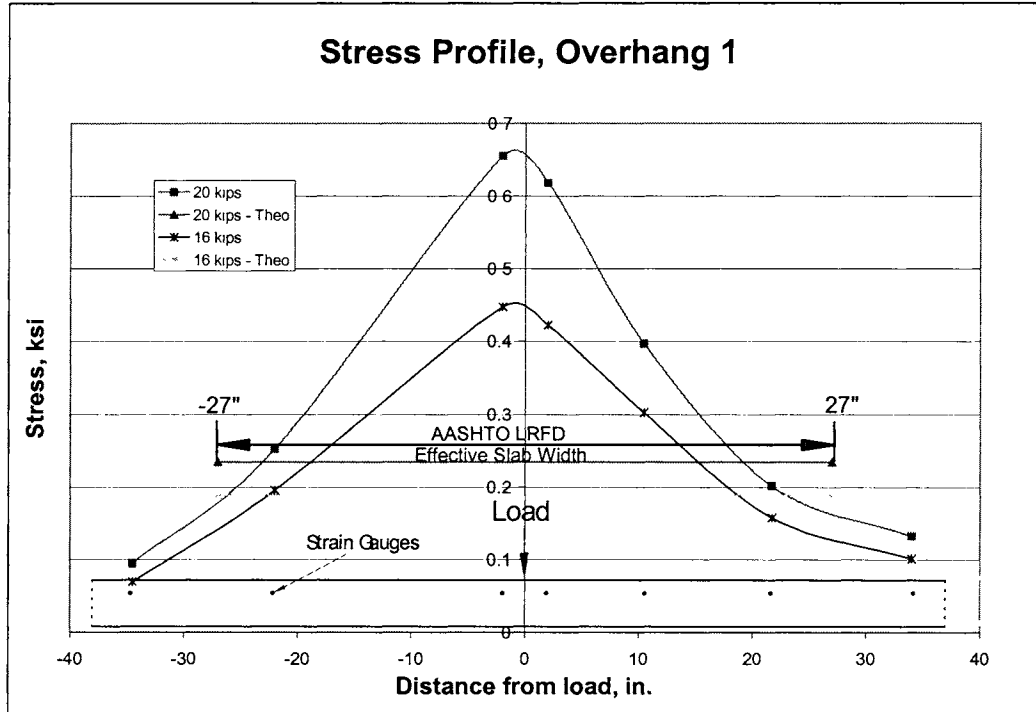


Figure 24. Stress profile, Overhang 1, before cracking.

Figure 24 also contains calculated theoretical values for the stresses in the bars. These were calculated by multiplying the effective load by a moment arm of 11 in to obtain an effective moment per foot width of slab. Since the section was not cracked at these two loads, the moment was multiplied by y , the distance from the bar to the neutral axis, 1.935 in, divided by the transformed moment of inertia, I_t , and multiplied by the modular ratio. The theoretical stress is plotted over the 4½ ft effective width and should match the peak stresses in the measured data, but it is significantly less. This indicates that for precracking loads, the effective width should be smaller. However, it must also be noted that the precrack stresses are extremely small and not an issue in design.

Figure 25 is the same type of stress profile, only at higher loads of 34 kips and 38 kips. This is considered to be after the section had cracked based on observations and data. The same pattern of high stresses closer to the loads is seen in this plot. The theoretical stresses were calculated in the same manner as before, only this time, the cracked moment of inertia, I_{cr} , was

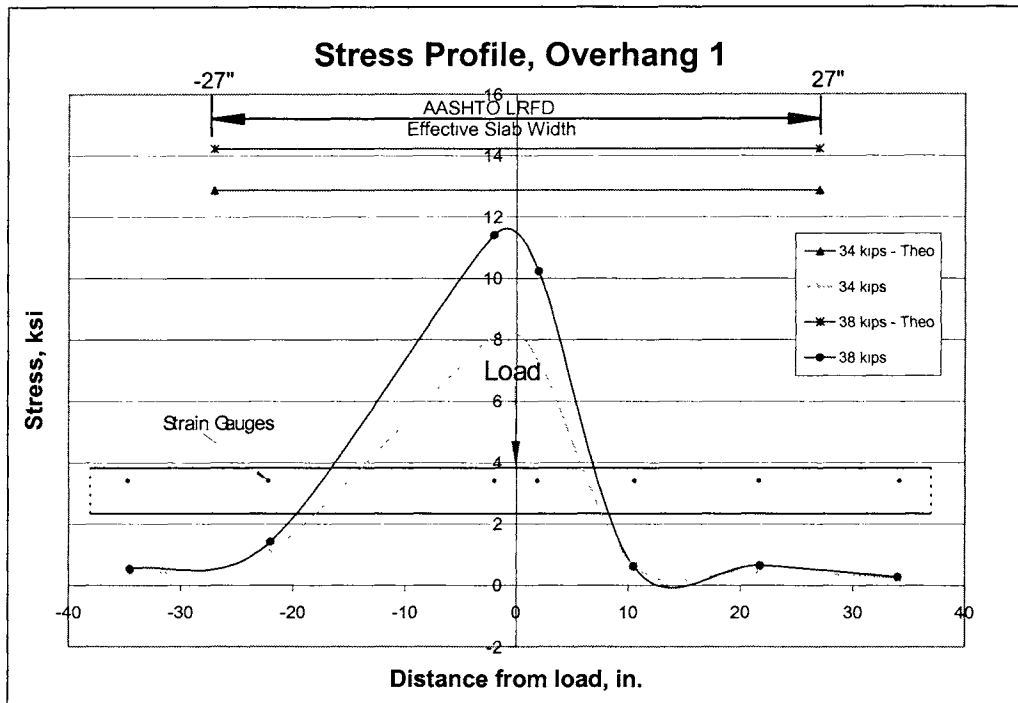


Figure 25. Stress profile, Overhang 1, after cracking.

used and the y value increased to 4.735 in. Now, the theoretical values are conservative and over-predicting the measured stresses. This indicates the effective width is conservative for predicting bar stresses in cracked sections.

Overhang 2

Figure 26 shows the load vs. strain plot for steel gauge 7. The plot initially has a constant negative slope up to a load of 20 kips. At 22 kips, the slope becomes positive and the strains gradually become tensile. This shows that the bar was initially below the neutral axis and in compression. At 22 kips, the section cracked, lowering the neutral axis and the compressive force in the bar decreased. The bar eventually went into tension, at which point the neutral axis was below the bar.

Figure 27 is a load vs. strain plot for GFRP gauges 37 and 38. Both gauges act similarly, but 38 has higher strains as the load increases, which is expected because it is closer to the load. They both have the same slope up to about 10 kips, where the slope of 38 changes slightly. Both slopes decrease slightly again at about 16 kips and then again more noticeably at 22 kips. This would correspond to some possible microcracking of the section and then visible cracking around 22 kips. The slope changes again around 32 kips, this time a drastic change, as the section has become significantly cracked.

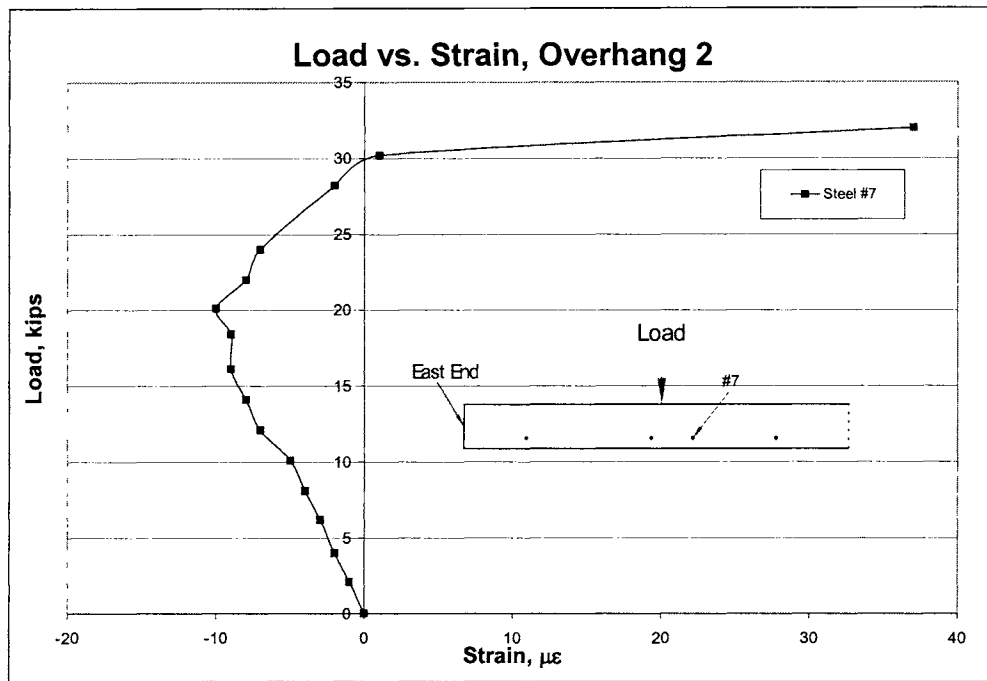


Figure 26. Load vs strain for Overhang 2, steel gauges.

The stresses were calculated by multiplying the strains by the modulus of elasticity. Stress profile plots were constructed similarly to those of Overhang 1. Figure 28 is a plot of the stresses at loads of 6.2 kips and 8.1 kips prior to visible cracking. The plot has the same trend as the plots for Overhang 1, with the stresses being higher closer to the load and tapering off with increased distance from the load. The theoretical stresses were calculated in the same manner and were plotted over the same effective width of 4½ ft. The effective moment was multiplied by a y of 1.81 in, divided by I_t , because the section was not considered to be cracked yet, and multiplied by the modular ratio. The theoretical approach predicts the peak stresses quite well.

Figure 29 is the same type of stress profile plot for the post-cracking loads of 34 kips and 40 kips. Again, higher stresses exist closer to the load and fall off with increased distance. The theoretical stresses were calculated using I_{cr} and a value of 4.62 in for y . As seen in the plot, the theoretical stresses are higher than the measured values; therefore, these values are considered to be conservative. The calculated stresses become less conservative with increased load. This is because the stresses are calculated assuming that the section is cracked across the full effective width, which is not initially the case. The section is only beginning to crack and as the load increases, the cracks in the section propagate deeper and wider and the measured values begin to approach the calculated values.

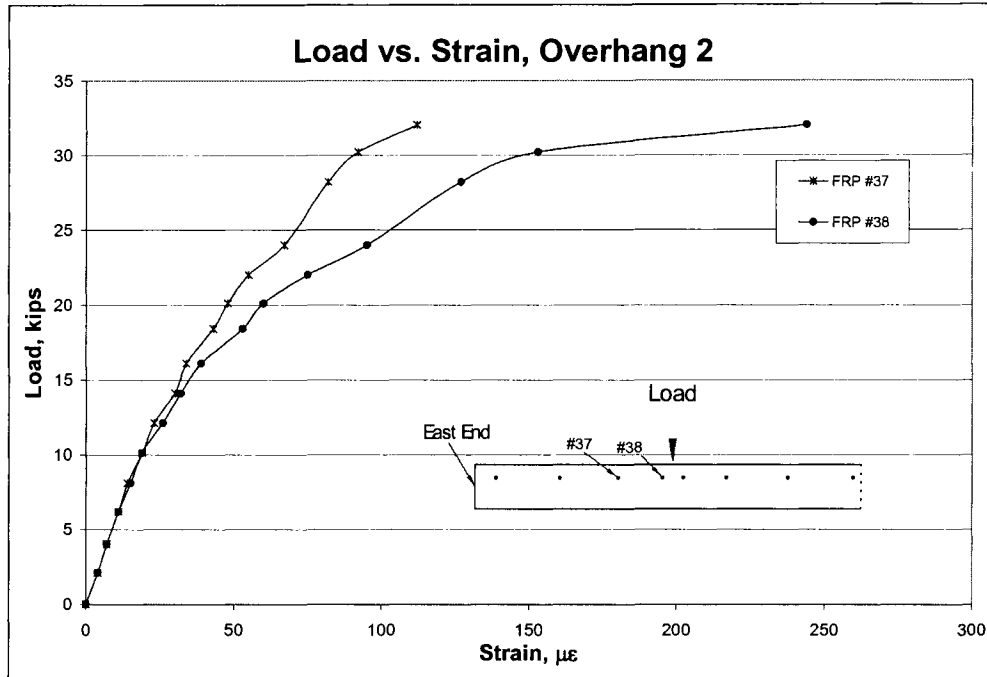


Figure 27. Load vs. strain, Overhang 2, GFRP gauges.

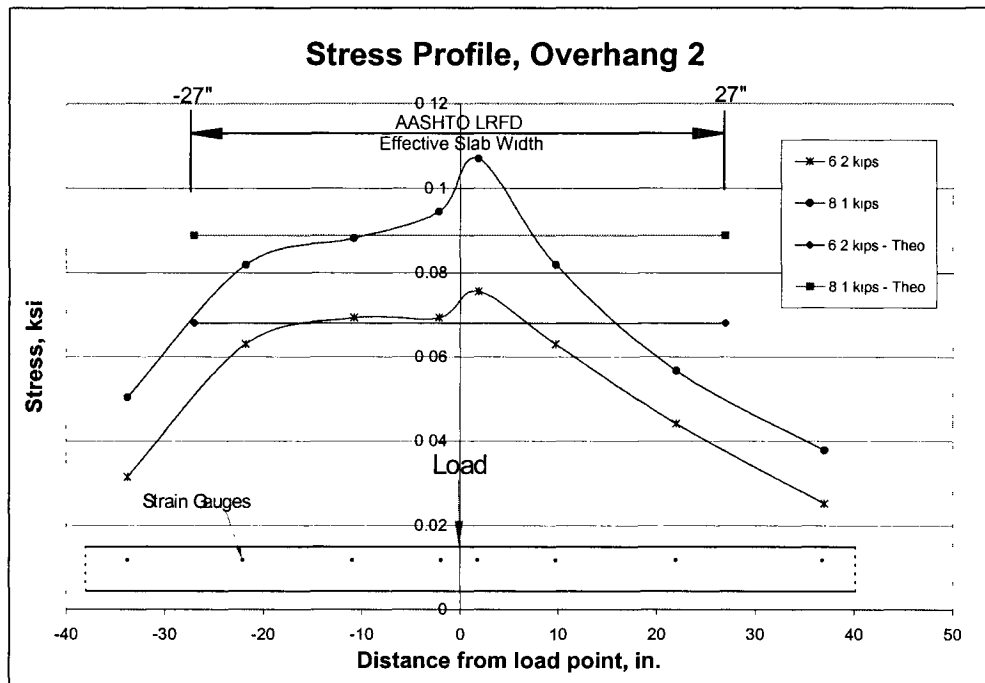


Figure 28. Stress profile, Overhang 2, before cracking.

Crack Widths and Cracking Loads

The first visible cracks occurred at a load of 28 kips for Overhang 1 and a load of 26 kips for Overhang 2. Cracking of the two overhangs then progressed in a similar manner. Figures 30 and 31 are crack maps of Overhang 1 and Overhang 2, respectively.

For Overhang 1, cracking started near the load and gradually progressed outward in a semicircular pattern. The first few cracks in Overhang 2 started further away from the load when compared to the first cracks in Overhang 1, but the pattern and progression were virtually the same.

As mentioned previously, the first visible crack in Overhang 1 was seen at a load of 28 kips. This is fairly consistent with the strain and deflection data, which indicated cracking at about 24 kips to 26 kips. The AASHTO LRFD effective width for overhangs and the cracking moment were used in conjunction to try to predict this first cracking load. With the cracking moment, M_{cr} , previously calculated as 6.47 ft-kips and the effective width calculated as 4.5 ft, the applied load needed to crack the section was calculated by multiplying M_{cr} by the effective width and then dividing by the moment arm of 11 in. This yielded an estimated cracking load of 31.8 kips, which is greater than the observed cracking load of 24 to 26 kips obtained from the strain and deflection data.

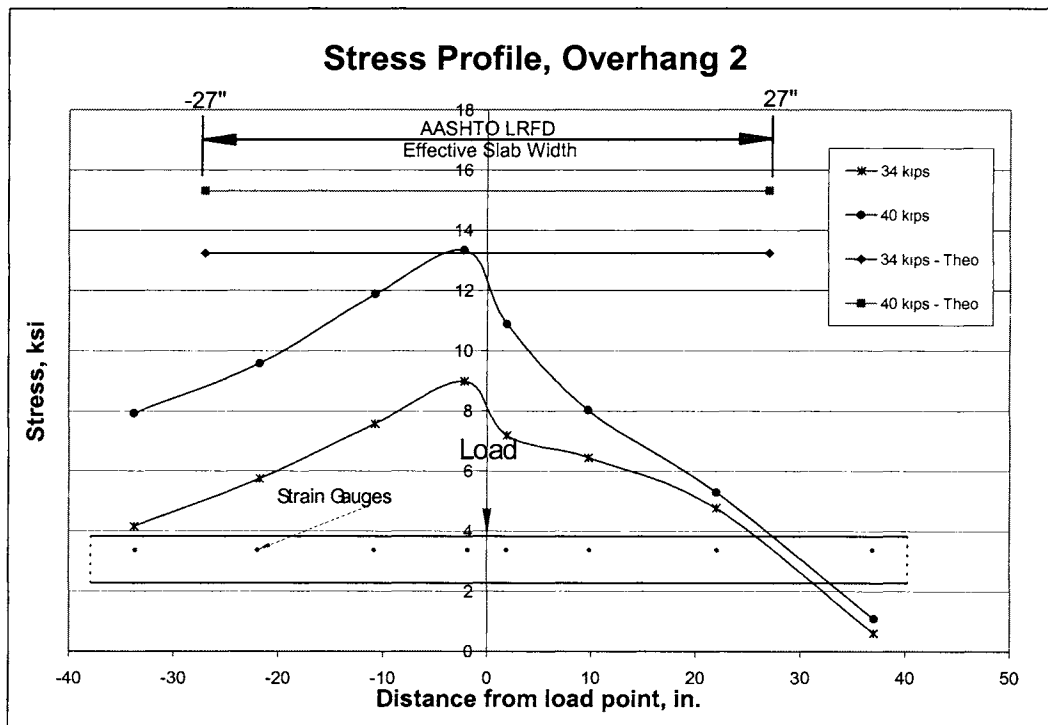


Figure 29. Stress profile, Overhang 2, after cracking.

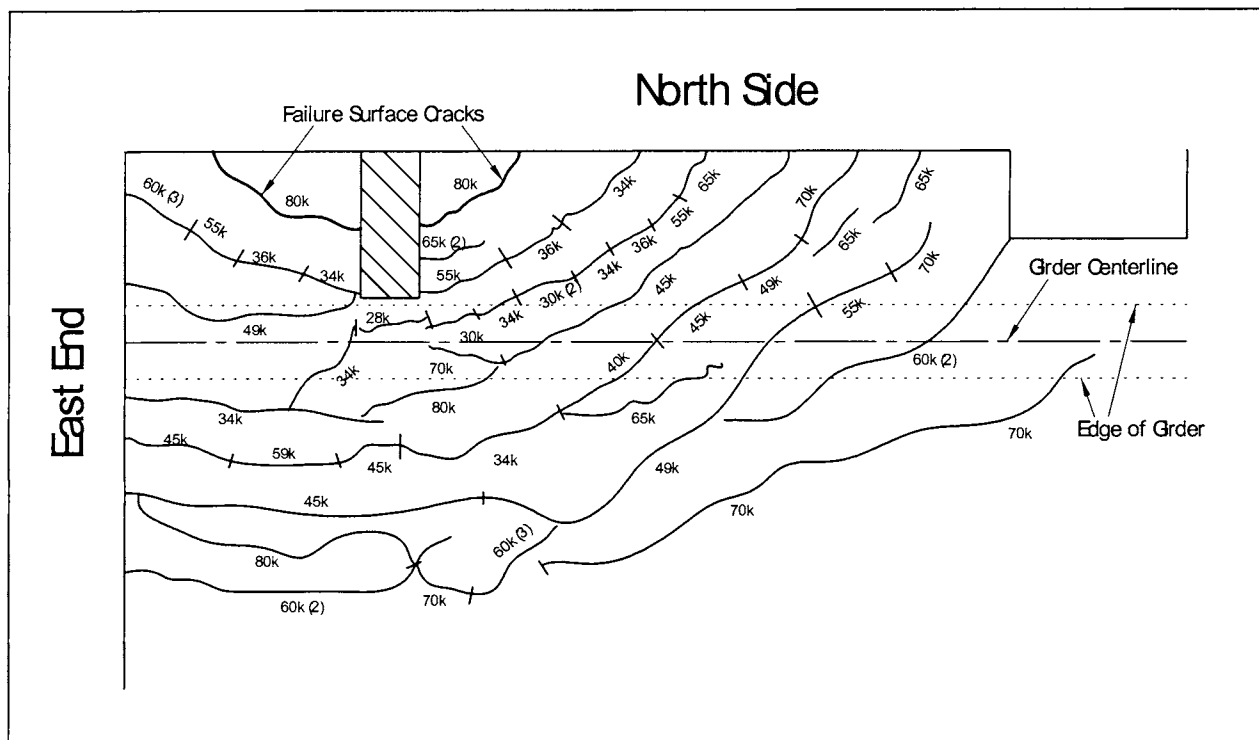


Figure 30. Crack map for Overhang Test 1.

Another method available for prediction of first cracking loads is to use influence surfaces for a plate or slab. Pucher (1977) created influence surface maps for a variety of support conditions, which for the overhangs case is a restrained edge of a cantilever (see Figure A.1 in Appendix A). To use the influence surface maps, the load is placed on the map and the value of the influence surface at that point is interpolated. This value is then divided by 8π and multiplied by the load to obtain the moment at the support. In this case, the moment to be found is at the edge of the girder, and the cantilever length is 21 in. The load is applied 11 in from the edge of the girder corresponding to a value of 9.1 on the influence map. With a calculated cracking moment of 6.47 ft-kips, the load to crack the section can be calculated by multiplying M_{cr} by 8π and dividing by 9.1. This yields a cracking load of 17.9 kips, which is lower than the observed cracking load of 24 kips to 26 kips.

Visible cracks did not appear on Overhang 2 until a load of 26 kips was reached. The strain and deflection data indicate that non-visible cracking probably occurred at a load of 22 kips. The AASHTO LRFD effective width and the influence surface methods both yield the same cracking loads as for Overhang 1 of 31.8 kips and 17.9 kips, respectively. These numbers once again over-predict and under-predict the actual cracking load of 22 kips. However, for Overhang 2, the influence surface method was closer to the observed cracking load.

As can be seen in Table 7, the ACI 440 equation predicts crack widths larger than the measured values, illustrating that for slabs the equation can be extremely conservative. One factor that may make the equation so conservative is f_f . This stress in the GFRP bars is calculated using the AASHTO LRFD effective width. In the previous section it was shown that this method over-predicts the stresses after the section cracks. This results in the crack widths being over-predicted as well.

Table 7. Measured and Calculated Crack Widths

Overhang 1 Crack Widths			Overhang 2 Crack Widths			
Load, kips	Measured, in.	Calculated, in.	Load, kips	Crack Card, in.	Whittemore, in.	Calculated, in.
28	0.002	0.0279	30	*	0.0014	0.0320
30	0.002	0.0302	32	0.013	-	0.0342
34	0.01	0.0341	36	0.016	0.0136	0.0385
36	0.013	0.0362	40	0.02	0.0188	0.0427
38	0.013	0.0378	45	0.02	-	0.0482
40	0.016	0.0401	50	0.04	0.0328	0.0534
45	0.016	0.0453	55	0.05	-	0.0587
49	0.02	0.0487	60	0.05	0.0558	0.0641
55	0.03	0.0550				
59	0.03	0.0600				

Ultimate Load and Failure Mode

The failure mode of both overhang tests was two-way shear, commonly referred to as punching shear. Overhang Test 1 failed at a load of 86 kips, and Overhang Test 2 failed at a slightly lower load of 78 kips. The failure mode and load were not predictable with calculations. The predicted failure mode was one-way shear. Equation 7, as presented in ACI 440 (ACI 2001), for the shear strength of concrete reinforced with FRP is shown here.

$$V_{c,f} = \frac{\rho_f E_f}{90 \beta_1 f_c'} 2\sqrt{f_c' b_w d} \quad (7)$$

Where : $V_{c,f}$ = nominal shear strength provided by concrete with FRP flexural reinforcement, lb

$$\rho_f = \text{FRP reinforcement ratio, } \frac{A_f}{b_w d}$$

A_f = area of FRP reinforcement, in²

E_f = modulus of elasticity of FRP, psi

f_c' = compressive strength of concrete, psi

b_w = width of web, in

d = depth to tension reinforcement from surface, in

β_1 = concrete factor equal to 0.80 for $f_c' = 5,000$ psi

With an A_f of 0.93 in², an E_f of 6,300,000 psi, an f_c' of 5,010 psi, a b_w of 12 in, and a d of 6.125 in, the shear capacity of Overhang 1 was calculated to be 2.3 kips per foot. This multiplied by the effective width of 4.5 ft yields a load of 10.3 kips. All of the parameters were the same for Overhang 2 except d was 6 in, which also yielded a shear failure load of 10.3 kips. Because the section did not fail in one-way shear as expected, the accuracy of this equation cannot be validated or disproved, but it does appear to be very conservative. This is probably a combination of the actual equation being conservative and the effective width equation being slightly conservative.

Equation 8 from ACI 318 (ACI 1999) was used to calculate the two-way shear capacity of the overhangs.

$$V_c = \left(2 + \frac{4}{\beta_c} \right) \sqrt{f_c'} b_o d \quad (8)$$

Where : V_c = nominal shear strength provided by concrete, lb

f_c' = compressive strength of concrete, psi

b_o = perimeter of critical section for slabs, in

d = depth to tension reinforcement from surface, in

β_c = ratio of long side to short side of concentrated load

With a β_c of 2.5, a b_o of 56.125 in, a d of 6.125 in, and an f_c' still equal to 5,010 psi, the two-way shear strength of Overhang 1 was calculated to be 87.7 kips, which is very close to the actual failure load of 86 kips. For Overhang 2, with a b_o equal to 56 in and a d of 6 in, the shear strength was calculated to be 85.7 kips. This is still relatively close to the actual failure load of 78 kips. Overall, it appears that the equation for punching shear predicts the failure loads for both overhangs reasonably well.

Design Criteria

Table 8 shows a comparison among allowable, calculated, and measured values for various design criteria.

Table 8. Design Criteria for Overhang Tests

Design Criteria	Overhang 1			Overhang 2		
	Allowable	Measured	Calculated	Allowable	Measured	Calculated
Stresses, ksi	12.1	1.87	7.92	12.1	3.55	8.01
Crack widths, in	0.02	<0.001	0.021	0.02	<0.001	0.022
Deflections, in	0.07	0.048	0.032	0.07	0.073	0.033
Nominal Capacity, k, based on:	Flexure	-	132	-	-	126
	One Way Shear	-	10.3	-	78	10.3
	Two Way Shear	-	87.7	-		85.7

The allowable stresses were calculated in accordance with the ACI 440 (ACI 2001) guidelines. For cyclic stress limits in FRP reinforcement, the allowable stress is 20% of the design tensile strength, f_{fu} . The design tensile strength, f_{fu} , is equal to the guaranteed tensile strength, f_{fu}^* , times an environmental reduction factor, C_E , which is equal to 0.7 for GFRP bars. The guaranteed tensile strength, f_{fu}^* , is equal to the tested average, 106 ksi for the No. 5 bars, minus three standard deviations of 6.68 ksi. This yielded a design value of 12.1 ksi. The measured values were taken at service load, 16 kips plus an impact factor of 30%, for a total load of 21 kips on the overhang. As can be seen in the table, the measured values for both overhangs are well below the allowable design value. This indicates that the design is conservative.

The calculated values for the crack widths were obtained using Equation 6. The load used for the calculation was 21 kips, a service load of 16 kips plus a 30% impact factor. ACI 440 (ACI 2001) recommends a maximum crack width of 0.02 in. In the two overhang tests, the slab was not cracked at a load of 21 kips. After the slab became cracked and a load of 21 kips was re-applied, the cracks were too small to measure and were less than 0.001 in when compared to a crack card. This indicates that the design method is conservative.

AASHTO LRFD Bridge Design Specifications (1998) set the recommended, not mandatory, allowable deflections at service loads of an overhang section as the length of the overhang section divided by 300. Overhangs 1 and 2 had a cantilever length of 21 in leading to an allowable deflection of 0.07 in at a service load of 21 kips. The measured data for Overhang 1 was well below the allowable, whereas the measured value for Overhang 2 was slightly higher. Overhang 1 indicates that the design is conservative, but Overhang 2 indicates that the design is neither conservative nor unconservative.

The nominal moment capacity of the section was calculated using Equations 9, 10, and 11, as presented in ACI 440 (ACI 2001) and shown here.

$$M_n = A_f f_f \left(d - \frac{a}{2} \right) \quad (9)$$

Where : M_n = nominal moment capacity of section, in - lb

A_f = area of FRP reinforcement, in²

f_f = stress in the FRP reinforcement in tension, psi

d = depth to the tension reinforcement from surface, in

a = depth of equivalent rectangular stress block, in

$$a = \frac{A_f f_f}{0.85 f_c' b} \quad (10)$$

Where : f_c' = compressive strength of concrete, psi

b = effective width of concrete, in

$$f_f = \left(\sqrt{\frac{(E_f \epsilon_{cu})^2}{4} + \frac{0.85 \beta_1 f_c'}{\rho_f} E_f \epsilon_{cu} - 0.5 E_f \epsilon_{cu}} \right) \leq f_{fu} \quad (11)$$

Where : E_f = modulus of elasticity of FRP, psi
 ϵ_{cu} = ultimate strain of concrete, 0.003
 ρ_f = FRP reinforcement ratio
 β_1 = concrete factor equal to 0.80 for $f_c' = 5,000$ psi
 f_c' = compressive strength of concrete, psi
 f_{fu} = design tensile strength of FRP, psi

The calculated nominal load based on flexure presented in Table 8 is the calculated nominal moment divided by the moment arm of 11 in. As can be seen, the section failed well before the nominal moment capacity was reached; therefore, the flexure design of the overhang does not control.

Interior Girder Test

Introduction

The test of the bridge deck over the interior girder was instrumented to gather deflection information, GFRP reinforcing bar stresses, cracking loads, crack widths, and failure load and type. The results of this test are presented in the following sections.

Deflections

With the wire pots anchored to the bottom of the slab, the deflections were measured at various load intervals. The data were collected, and load vs. deflection plots were made. Figure 32 presents the load vs. deflection curves measured for two of the wire pots and one theoretical load-deflection curve. The locations of the two wire pots are shown in the figure. Both were under the patch load 3 ft 3 in on either side of the interior girder.

The theoretical deflections were calculated similarly to the Theo. I_{eff} method for Overhangs 1 and 2. The effective width for this case was calculated using Equation 12 as presented in Table 4.6.2.1.3-1 of the *AASHTO LRFD Bridge Design Specifications* (1998), and shown here:

$$EW_{neg.mom.} = 48in + 0.25S \quad (12)$$

Where : $EW_{neg.mom.}$ = effective width of negative moment region, in
 S = spacing of supporting components (girders), in

The effective width was found to be 5 ft 7½ in. The deck was again modeled as a 12-in-wide strip in the analysis program RISA-2D (RISA 1993) with the girders modeled as pin supports. The overhang portions were not included in the analysis as they have no effect on the deflections due to applied loads. Two equal loads were applied, one 3 ft on either side of the interior girder.

The loads applied in the analysis were equal to the applied test loads divided by the effective width of the overhang, to obtain an effective load on a 12-in strip.

The analysis was performed using an effective moment, I_e , over the whole section. This effective moment of inertia was a combination of two moments of inertia, the midspan effective moment of inertia, $I_{e(m)}$, and the support effective moment of inertia, $I_{e(l)}$. Both of these were calculated using Equations 3 and 4 as presented previously, using the transformed moment of inertia, I_t , as opposed to the gross moment of inertia, I_g . They were combined using Equation 13 for beams continuous on only one end as prescribed by ACI 435 (ACI 1995).

$$I_e = 0.85 I_{e(m)} + 0.15 I_{e(l)} \quad (13)$$

Where: I_e = effective moment of inertia, in^4

$I_{e(m)}$ = effective moment of inertia at midspan, in^4

$I_{e(l)}$ = effective moment of inertia at the support, in^4

Each effective moment of inertia had a different M_{cr} and M_a . The M_a for each was calculated using the RISA-2D (RISA 1993) analysis program. M_{cr} for each was calculated using Equation 5, with f'_c equal to 5770 psi. This was the average compressive strength of batch 1 and 2 combined at 64 days. This was used because the region of the slab involved in the test contained concrete from batches 1 and 2 and the test was performed just before the 64-day break. $M_{cr(m)}$ was calculated as 5.75 k-ft per ft, and $M_{cr(l)}$ was calculated as 5.48 k-ft per ft. I_e for the section was equal to I_t , 443.3 in^4 , up to the load of 50 kips. At this load, $M_{a(l)}$ exceeded $M_{cr(l)}$, so the section was assumed to be cracked at the interior support. $I_{e(m)}$ was equal to I_t up to a load of 80 kips. At 80 kips, the section was assumed to be cracked over the support and at midspan.

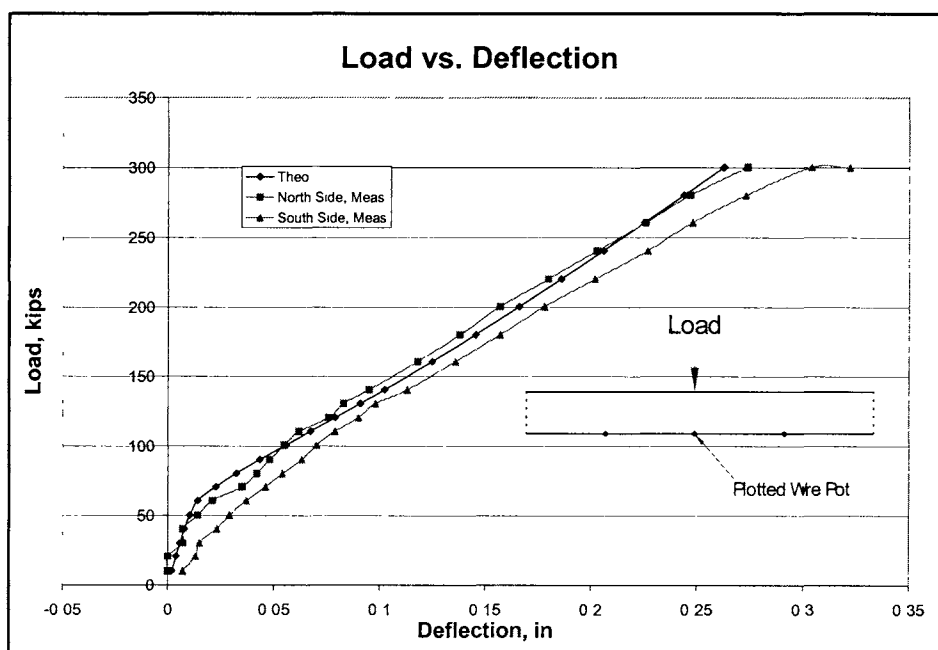


Figure 32. Load-deflection plot for interior girder test.

As shown in Figure 32, the theoretical method predicts the measured deflections of both wire pots very well. The theoretical method predicts the north side deflections slightly better than the south. At a load of 50 kips, the slope of the theoretical line starts to decrease, and by a load of 70 kips, the slope has decreased significantly. This same behavior can also be seen in the north side wire pot, though the first few data points are a little sporadic. The south side data, on the other hand, starts out with a lower slope than the other two, but a change in slope can still be seen around 50 kips. The change in slope of all the series indicates that cracking has occurred in the section. After a load of 70 kips, all three curves exhibit the same behavior. The two measured curves have slightly lower slopes than the theoretical at these higher loads. This is probably due to the fact that shear deformations are occurring and were not accounted for in the theoretical approach. Overall, it can be said that the effective width equation, the two effective moment of inertia equations, and the RISA-2D (RISA 1993) model predict the deflections very well.

Reinforcing Strains and Stresses

Figure 33 is a load vs. strain plot of steel strain gauge #13. The location of the gauge is shown in the plot. The slope of the plot is negative up to a load of 90 kips, indicating that the bar is initially below the neutral axis and is in compression. At 90 kips the slope begins to change and becomes positive at 110 kips. This indicates a crack in the section and the gradual lowering of the neutral axis. At 140 kips, the bar is in tension because the section has become cracked such that the neutral axis has dropped below the bar.

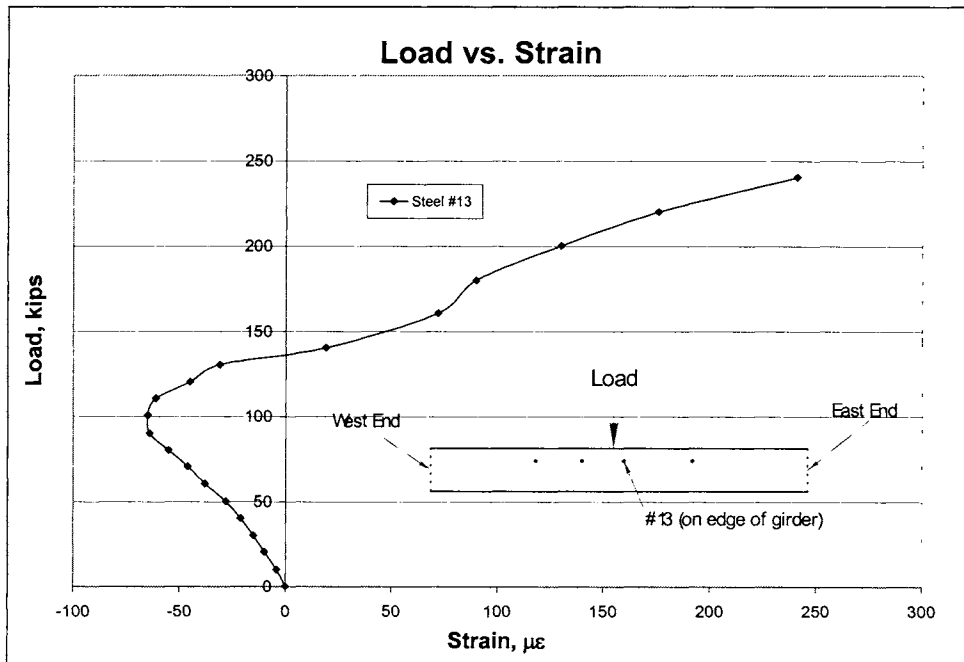


Figure 33. Load vs. strain, steel gauge, interior girder test.

Figure 34 is a load vs. strain plot of GFRP strain gauges # 49 and #50. Gauge #49 is on the south side of the girder, and #50 is on the north side of the girder. Both gauges exhibit the same behavior and have approximately the same strains up to a load of 50 kips. Both also have a slight slope change at 40 kips. At 60 kips, the slope of #49 decreases greatly, indicating a crack in the section and a lowering of the neutral axis. Gauge #50 has the same behavior, except at a load of 90 kips, also indicating a cracked section and lowering of the neutral axis. Also at 90 kips, the slope of #49 increases up to a load of 120 kips, and the strain in #49 and #50 are almost equal. At this point, the slope of #49 decreases again and has the same slope as #50. These changes in slope can be attributed to the stepwise onset of cracking and the redistribution of moments within the continuous slab.

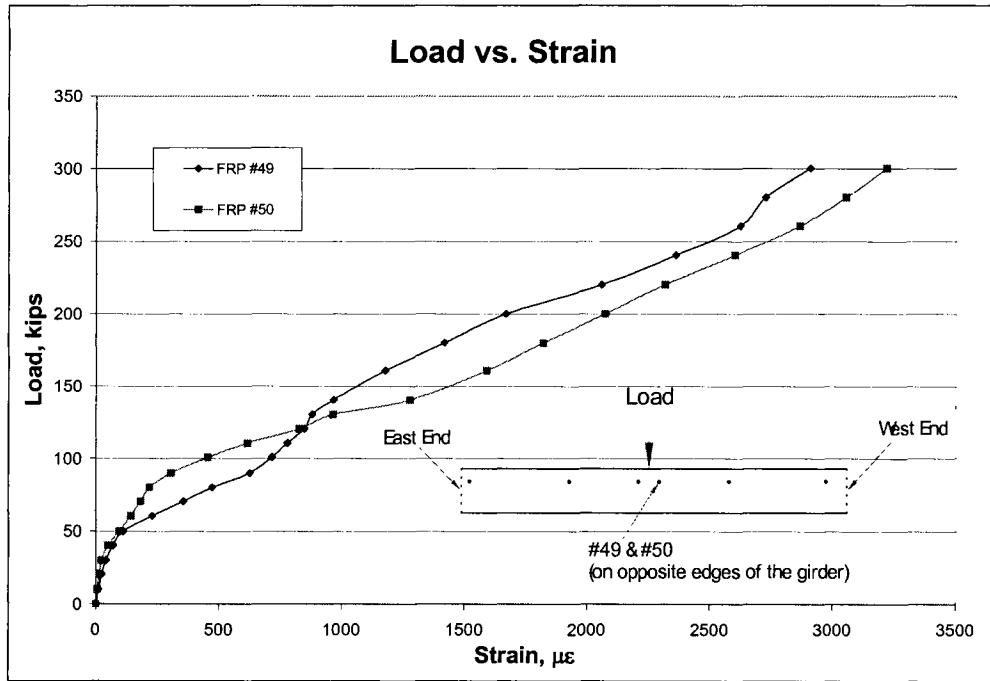


Figure 34. Load vs. strain, GFRP bars, interior girder test.

The stresses in the GFRP bars were obtained by multiplying the recorded strains by the modulus of elasticity of the GFRP bars, 6,300 ksi. Stress profile curves were then created at various loads. These plots showed the stress in each bar relative to its distance from the load point. Figure 35 is a stress profile plot for loads of 10, 20, and 30 kips prior to cracking. As can be seen and as expected, the stresses are high close to the load and taper off as gauges get further away from the load.

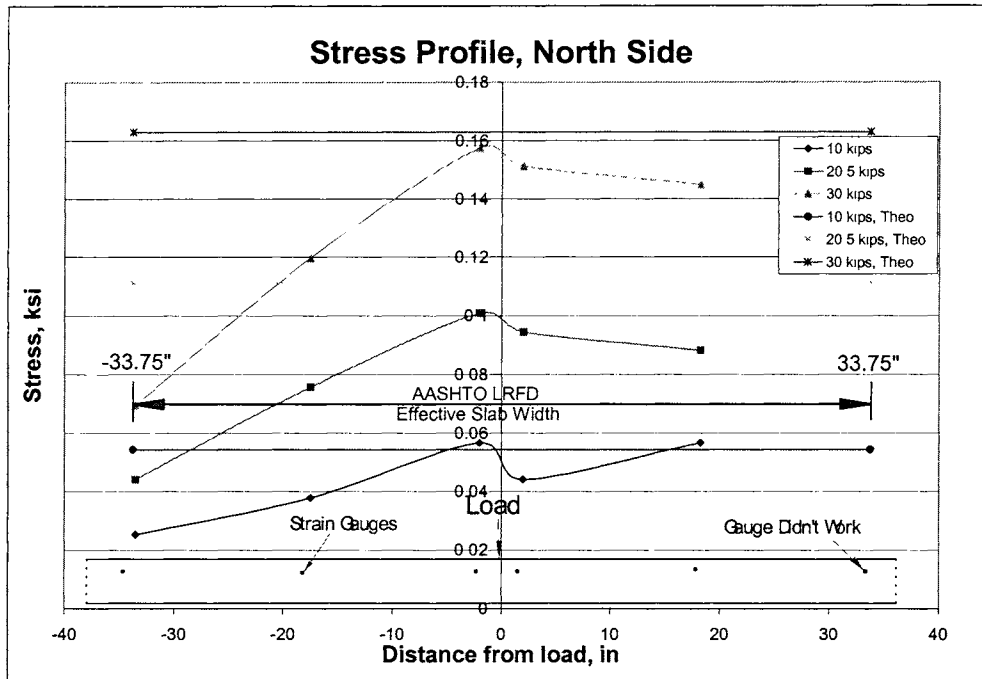


Figure 35. Stress profile of interior girder test, precracking.

Figure 35 also contains calculated stresses in the bars. These were calculated by using the effective moment at the edge of the girder flange found in the RISA-2D (RISA 1993) analysis. Since the section was not cracked at these three loads, the moment was multiplied by y , the distance from the bar to the neutral axis, 1.65 in, divided by the transformed moment of inertia, I_t , and multiplied by the modular ratio. The theoretical stress is plotted over the 5 ft 7½ in effective width and should match the peak stresses in the measured data. The calculated stresses are similar to the measured peak stresses. Note that the bar stresses are very low at precracking moments and are not an issue in design.

Figure 36 is the same type of stress profile, on the south side, at higher, post-cracking loads of 70, 80, and 90 kips. The same pattern of high stresses close to the loads is again seen in this plot. The theoretical stresses were calculated in the same manner as before, only this time, the cracked moment of inertia, I_{cr} , was used and the y value increased to 4.23 in. Now, the calculated stresses are considerably higher than the measured stresses. This is because the theoretical stresses are calculated assuming that the section is cracked over the full effective width when it is not. Another source of error is the calculation of moment at the section, which assumes a uniform slab stiffness over the full slab length.

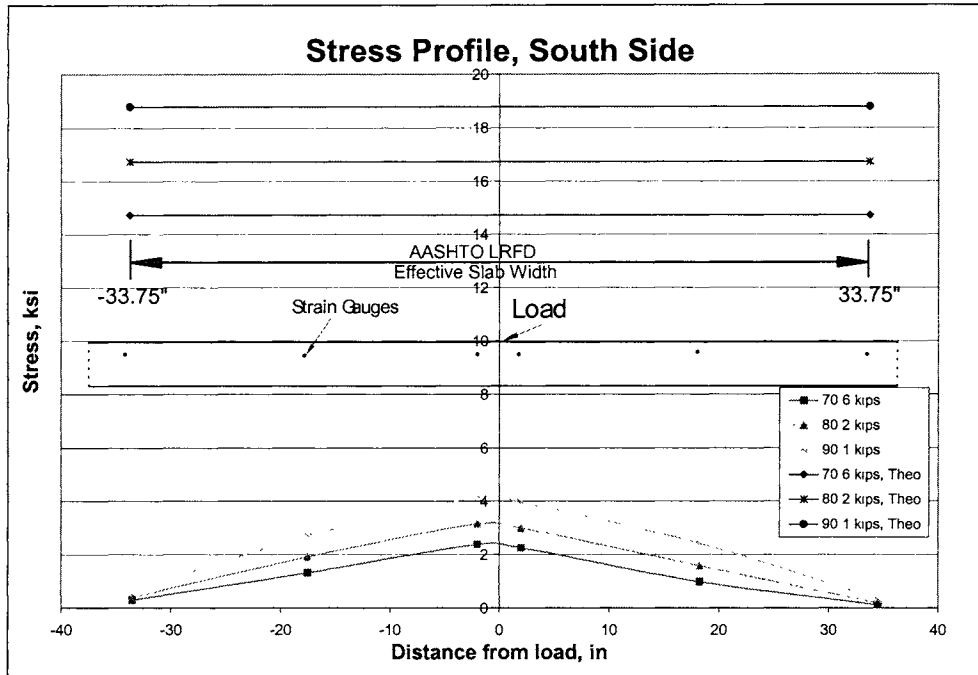


Figure 36. Stress profile of interior girder. after cracking.

Crack Widths and Cracking Loads

The first visible crack was seen at a load of 60 kips, 30 kips per patch. The cracks first appeared on the edge or near the edge of the interior girder flange close to the load. As the load increased, the cracks progressed along the edge of the flange toward either end of the deck. The progression and location of these cracks can be seen in Figure 37.

As mentioned, the first visible crack in the deck was seen at a load of 60 kips near the edge of the flange. This is consistent with the GFRP strain and deflection data, which also indicated cracking at about 60 kips. The AASHTO LRFD effective width for negative moment regions and the cracking moment were used in conjunction to try to predict this first cracking load. With the cracking moment over the support, $M_{cr(1)}$, previously calculated as 5.48 ft-kips and the effective width calculated as 5 ft 7½ in, the applied load to crack the section was calculated by dividing $M_{cr(1)}$ by the moment at the support from the output of the analysis program RISA-2D (RISA 1993) with 1 kip applied, ½ kip at each patch. That number was then multiplied by the effective width, and this yielded an estimated cracking load of 50 kips, 25 kips per patch, which is close to the observed cracking load, considering load was applied in 10-kip increments.

The measured and theoretical crack widths for the interior girder test are presented in Table 9. The crack widths were measured using a crack microscope, which is much more accurate than a crack card. The theoretical values were calculated using Equation 6, the ACI 440 (ACI 2001) modified Gergely-Lutz equation as described previously.

Table 9. Measured and Calculated Crack Widths

Load, kips	Measured Crack Width, in	Calculated Crack Width, in
60	0.0024	0.0324
70	0.0024	0.0378
80	0.0039	0.0429
90	0.0047	0.0482
100	0.0055	0.0538
120	0.0063	0.0644
140	0.0087	0.0752
160	0.0102	0.0860
180	0.0118	0.0963
200	0.0157	0.1068
220	0.0189	0.1178
240	0.0213	0.1287
260	0.0236	0.1394
280	0.0260	0.1500
300	0.0394	0.1607

Design Criteria

Table 10 shows a comparison among allowable, calculated, and measured values for various design criteria.

The allowable stresses were calculated in accordance with the ACI 440 (ACI 2001) guidelines. As explained for the overhang tests, the allowable stress for the GFRP bars is 12.1 ksi. The measured values were taken at service load, 32 kips plus an impact factor of 30%, for a total load of 42 kips on the deck. The presented measured values are at a load of 40 kips. As can be seen in the table, the measured stress is well below the allowable design value. The measurement was taken before the section had cracked and is expected to be low. The section was cracked at 60 kips, however, and the stress was 1.5 ksi, still well below the allowable stress. The allowable of 12.1 ksi was not reached until a load of 180 kips. This indicates that the design is conservative.

The crack widths were calculated using Equation 6. The load used for the calculation was 42 kips, a service load of 32 kips plus a 30% impact factor. ACI 440 (ACI 2001) recommends a maximum crack width of 0.02 in. In the test, the slab was not cracked until a load of 60 kips. After the slab became cracked at a load of 60 kips, the measured crack widths were still very small, 0.0024 in.

Table 10. Design Criteria for Interior Girder Test

Design Criteria	Interior Girder Test Values		
	Allowable	Measured	Calculated
Stresses, ksi	12.1	0.441	0.23
Crack Widths, in	0.02	Not cracked	0.022
Deflection, in	0.0975	0.023/0.007	0.0077
Nominal Capacity, kips based on:	Flexure	318	415
	One-way Shear		44
	Two-way Shear		214

AASHTO LRFD Bridge Design Specifications (1998) set the recommended, not mandatory, allowable deflections at service loads of a bridge deck as the spacing of the girders divided by 800. The spacing of the girders was 78 in leading to an allowable deflection of 0.0975 in at a service load of 42 kips. The measured data were for a load of 40 kips and was well below the allowable. Once again the section was not cracked, and therefore the deflections are expected to be small. However, at 60 kips with a cracked section, the deflection was still only 0.036 in. Allowable service deflections were not reached until a load of 130 kips.

The nominal moment capacity of the section was calculated following the same procedure described previously. The nominal moment capacity is 257.7 ft-kips, which equates to an applied load of 415 k. However, the section did not fail in flexure, it failed in punching shear. The punching shear capacity was calculated as 214 kips, which is considerably less than actual ultimate. Similarly to the overhangs, the one-way shear capacity as calculated with the ACI 440 (ACI 2001) equation predicts a very low failure load, which was not seen in the tests.

Cantilever Test

Introduction

The cantilever test models a negative moment region over an interior support in a continuous bridge. Measurements were taken to obtain deflection information, GFRP reinforcing bar stresses, cracking loads, and crack widths. The results of this test are presented in the following sections.

Deflections

Wire pots were attached to the bottoms of the girders with magnets. They were attached to the ends of the girders on the west end. The data were collected during the testing, and load vs. deflection plots were created. Figures 38 and 39 present the load-deflection plots for the interior and exterior girders. Both plots contain measured and calculated deflections. The measured deflections for both beams are very similar. Both follow a fairly straight line, and no significant slope change is seen. They both do have a small plateau at a load of 110 kips. This is because the bridge was loaded up to 110 kips, unloaded and cycled between 10 kips and 80 kips 5 times, and then reloaded up to 110 kips. At the second load of 110 kips, the section had softened somewhat and deflected a little more than the first time, leading to a plateau in the plot.

The theoretical deflections for the interior and exterior girders were calculated the same way. The system was modeled as a beam element in RISA-2D (RISA 1993) and was loaded with the applied test load. The only difference in the modeling of the interior and exterior beams was the location of the supports. Both had roller supports 4 ft from the load, and both had pin supports 20 ft from the load. The two exterior girders had no other supports; however, the interior girder had a pin support 12 ft from the load where it was bolted down to the reaction floor. To model the sections as beams, the transformed moments of inertia of each section were calculated considering the composite action between the slab and the girders. The effective flange widths of the slab were calculated for the interior and exterior beams using Equations 14 and 15 as presented in the *AASHTO LRFD Bridge Design Specifications* (1998).

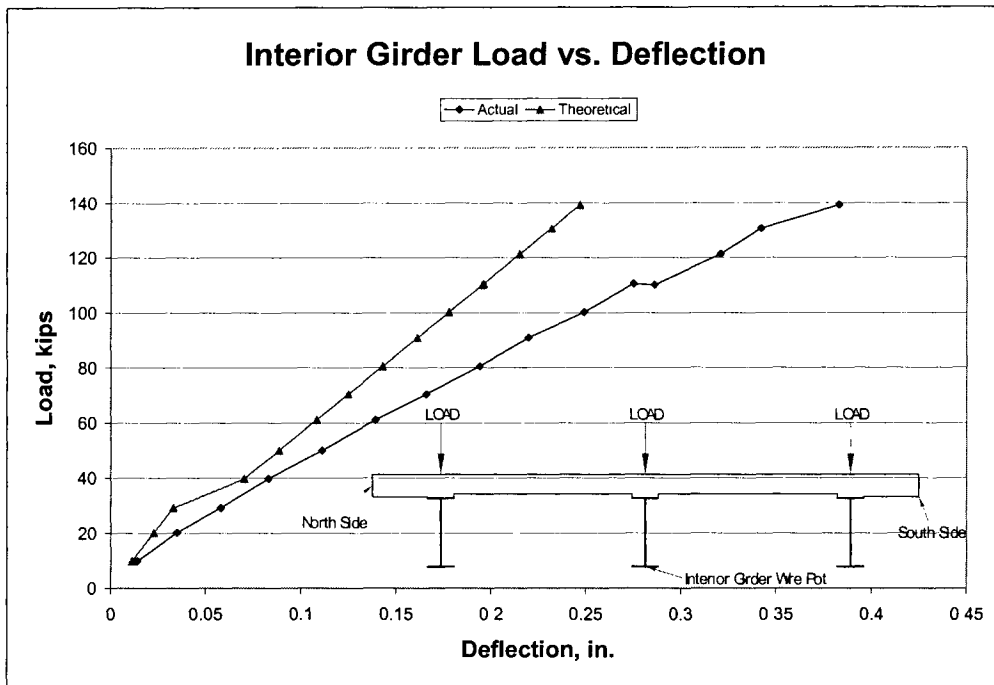


Figure 38. Load-deflection plot for interior girder, cantilever test.

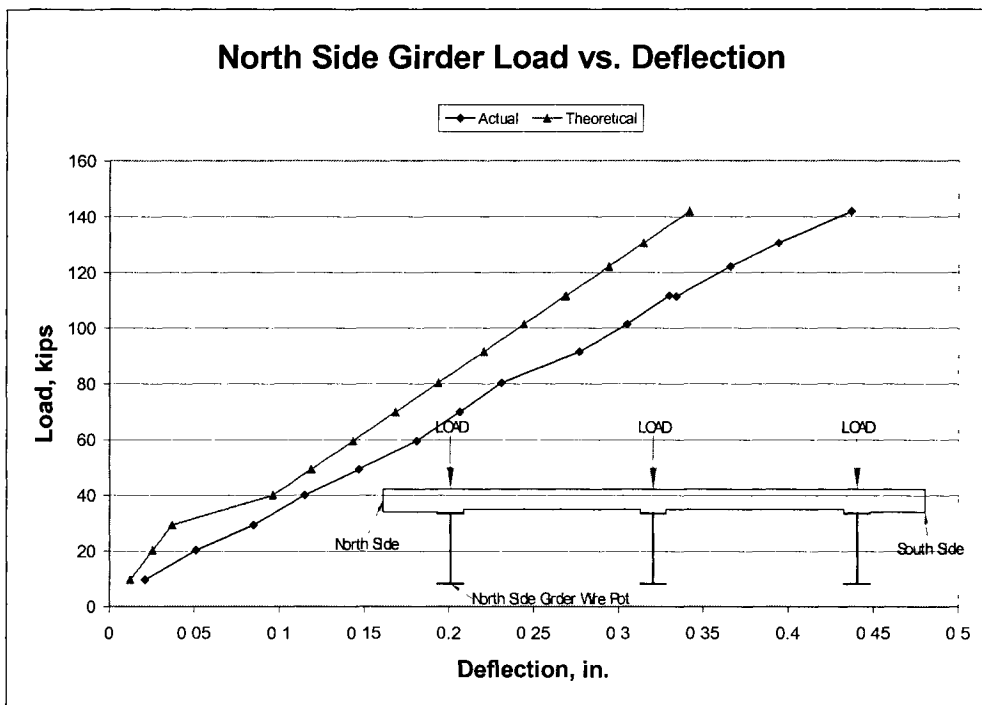


Figure 39. Load-deflection plot for exterior girder, cantilever test.

$$b_i \leq \left\{ \begin{array}{l} \frac{1}{4} \text{ effective span} \\ 12t_s + \frac{1}{2} b_f \\ \text{ctr. to ctr. spacing of girders} \end{array} \right\} \quad (14)$$

Where : b_i = effective width for interior girders, in
 t_s = thickness of slab, in
 b_f = width of top flange of girder, in

$$b_e - \frac{b_i}{2} \leq \left\{ \begin{array}{l} \frac{1}{8} \text{ effective span} \\ 6t_s + \frac{1}{4} b_f \\ \text{width of overhang} \end{array} \right\} \quad (15)$$

Where : b_i = effective width for interior girders, in
 b_e = effective width for exterior girders, in
 t_s = thickness of slab, in
 b_f = width of top flange of girder, in

For the interior girder, the center-to-center spacing of the girders governed and the effective width was calculated to be 78 in. For the exterior girders, the width of the overhang governed and the effective width was calculated to be 65 in. The transformed moments of inertia were calculated for both. The GFRP and concrete areas were transformed to steel by using the materials' modular ratios. The cracked moments of inertia were also calculated for both, discounting the presence of any concrete and again transforming the GFRP to steel.

The transformed moment of inertia, I_t , for the interior girder was calculated to be 11,184 in⁴, with the neutral axis located 27.9 in from the bottom of the girder. The cracked moment of inertia, I_{cr} , for the interior girder was calculated to be 4346 in⁴, with the neutral axis located 15.63 in. from the bottom of the girder. The exterior girders had a transformed moment of inertia of 10,797 in⁴, with the neutral axis located 27.5 in from the bottom of the girder, and a cracked moment of inertia of 4273 in⁴, with the neutral axis located 15.5 in from the bottom of the girder. See Appendix B for example calculations.

The transformed moments of inertia were used in the analysis program up to a load of 30 kips. At a load of 40 kips, the cracked moment of inertia was used because based on observations, this is the load at which the deck cracked. The deflections were calculated for each load in the analysis program. In order to calculate the actual deflections at the ends of the girders, shear deformations of the girders had to be accounted for because in short spans such as this, shear deformations tend to be large. To account for the shear deformation, the beam

element in the RISA-2D (RISA 1993) model was modeled as a bare W27x94 steel girder, with the same supports and loads. The model was run once at each load including shear deformations and once not including shear deformations. The second run was subtracted from the first run to obtain the deflections due to just shear deformations. These deflections were then added to the corresponding deflections using the transformed and cracked moments of inertia to obtain the total theoretical deflection.

As seen in the figures, the theoretical deflections do not match the actual deflections precisely, but they are reasonably close. They are all less than the actual, which indicates that the theories and methods behind the calculations are somewhat unconservative. Both theoretical sections appear to be stiffer than their corresponding actual section up to a load of 30 kips because both have larger slopes. As mentioned, at 40 kips, the sections are modeled as cracked and there is a significant change in their slopes. This change in slope is not seen at all in the measured deflections section, which is quite unusual because the moment of inertia should be greatly reduced when the section cracks. Cracking should result in a less stiff section that will deflect more with the same load increment. Another difference between the actual and theoretical deflections is that the theoretical curve has a steeper slope after cracking as well. This shows once again that the model is stiffer than the actual section. Overall, the calculated deflections are smaller than measured. This discrepancy in deflections and stiffness may be due to a number of different things. They include shear deformations in the slab, deflection at the support, and loss of composite action between the slab and the girder.

Strains and Stresses in Girders and Reinforcing Bars

The strains were recorded using the data acquisition system, and load vs. strain plots were created. Figure 40 is a load vs. strain plot for the two strain gauges that were located on the south side girder close to the support. The data series labeled “top” was for the strain gauge located at the top of the girder, and the data series labeled “bottom” corresponds to the gauge located at the bottom of the girder. From the plot, it appears that the top strain gauge was located very close to, if not on, the neutral axis because it has 0, or close to 0, strain up to a load of about 50 kips. The bottom gauge is well below the neutral axis and is in compression. At 50 kips, in the top gauge, there is a very slight increase in the strain, and by 60 kips the strain has increased significantly and is well into tension. This shows that the section above the girder may have begun to crack at 50 kips and by 60 kips the cracking had progressed. At this point, the neutral axis was significantly lowered and the top strain gauge was well above it.

Figure 41 is a plot of load vs. strain for the two steel reinforcing bars located above the south side girder. They show the same pattern as seen in the south side girder top gauge, only they are located above the neutral axis initially and have a more positive slope to begin with. As can be seen, there is a slope change and strain increase at 50 kips and then a significant slope change and strain increase at a load of 60 kips, once again showing that the section may have begun to crack at 50 kips, thus dropping the neutral axis and increasing the strains in the steel reinforcing bars.

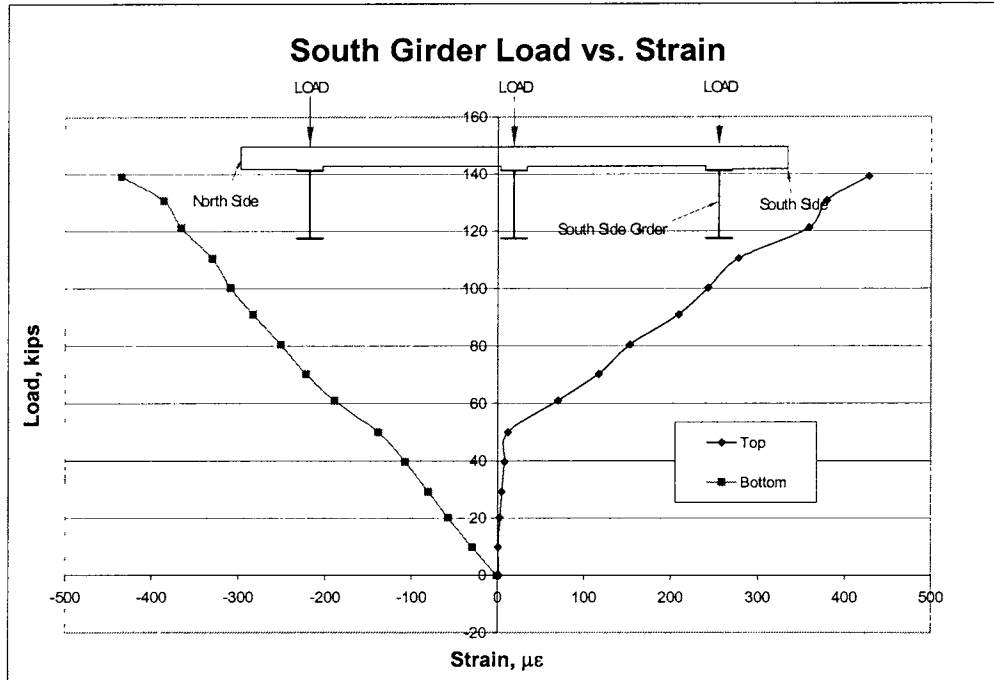


Figure 40. South girder load vs. strain.

Figure 42 is a load vs. strain plot for the GFRP stain gauges. The locations of the bars are shown on the plot. Each is located directly over the centerline of the three girders. All three have positive slopes and are initially in tension because they are located above their respective neutral axes. All three also have almost identical slopes and values up to cracking. The north girder section, which contains gauge #64, appears to crack first at a load of 30 kips, followed by the interior girder section containing gauge #60 cracking at 40 kips, and then the south side section beginning to crack at a load of 50 kips, as indicated by gauge #56. Gauge #56 is located above the south side girder, and its load-strain behavior is almost identical with the steel gauges in Figure 41, which is expected because it is located just above the steel gauges. It shows the same pattern of beginning to crack at 50 kips and then being significantly cracked at 60 kips. The increase in strains and decrease in slopes indicates that the section has cracked, the neutral axis has lowered, and the bars are taking more strain at equal load increments.

The stresses in the GFRP bars were obtained by multiplying the recorded strains by the modulus of elasticity of the GFRP bars, 6,300 ksi. Stress profile curves were then created at various loads. These plots showed the stress in the each bar relative to its distance from the load points. Figure 43 is a stress profile plot for loads of 30 and 40 kips. As can be seen and as expected, the stresses are high close to the beams and taper off as gauges get further away from the beams.

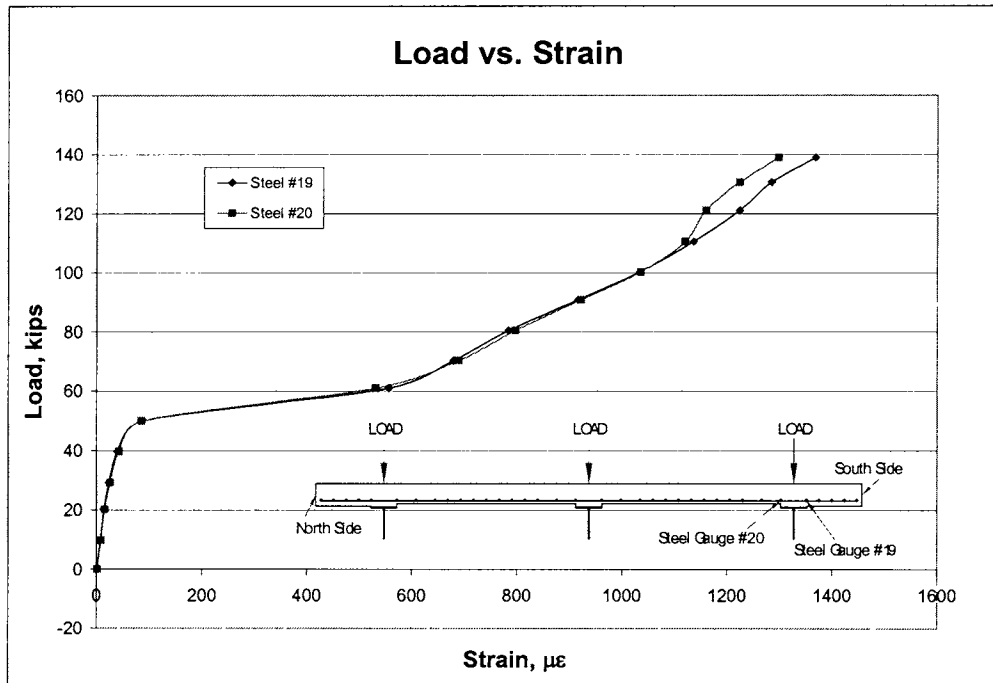


Figure 41. Steel reinforcing strains.

The plot also contains calculated stresses. These stresses were calculated by multiplying the moment at any given load by the appropriate distance from the bar to the neutral, y , and then dividing by the appropriate moment of inertia, I , and multiplying by the modular ratio. The moment was the applied load, 30 or 40 kips, times the moment arm of 48 in. A cracked moment of inertia and its corresponding y value were used for the north side girder at 30 and 40 kips and for the interior girder at 40 kips because the sections were determined, by observation, to be at least partially cracked at these loads. For the other cases, the interior girder at 30 kips and south side girder at 30 and 40 kips, the transformed moment of inertia and its corresponding y value was used.

The plot shows that the measured stresses are somewhat higher than calculated before the section first starts to crack. This first cracking occurred at a load of 30 kips for the north side section and 40 kips for the interior section. As can be seen on the plot, the calculated stresses are similar to the measured stresses for these two situations. However, at a load of 40 kips on the north side section, the actual stress reached about 6 ksi and the calculations predicted a stress of only about 1.7 ksi, which is about 30% of the actual. For the uncracked sections, the calculated stresses are slightly less than the measured stresses, which is of little concern because cracked sections are usually used in design and the stresses at this level are well below the allowable stress of 12.1 ksi.

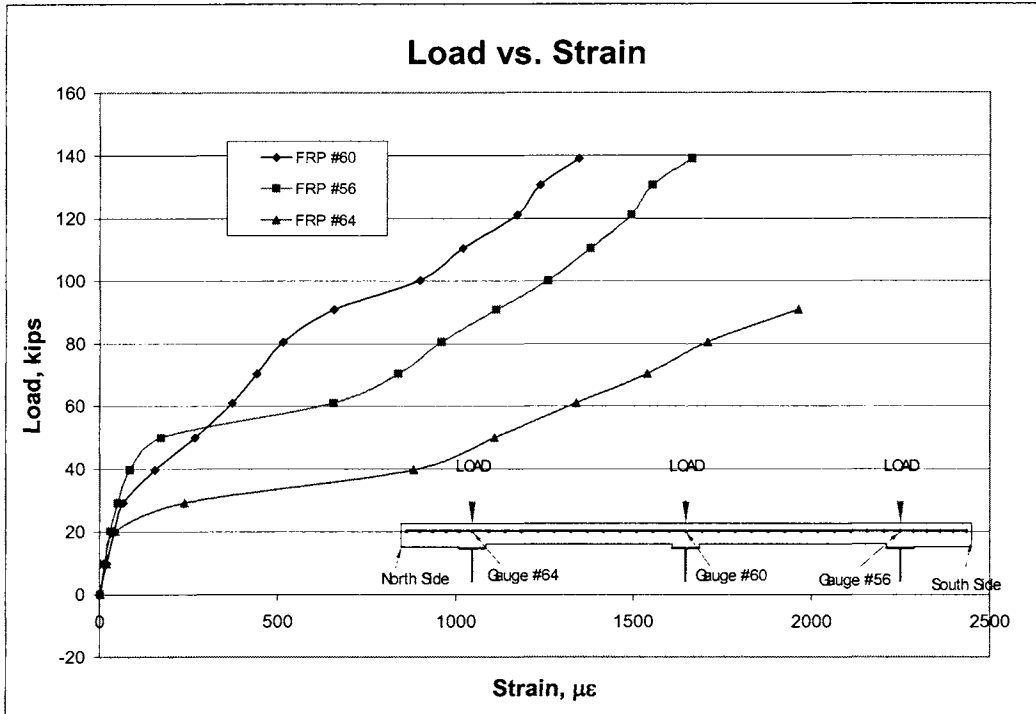


Figure 42. Load vs. strain for GFRP bars, cantilever test.

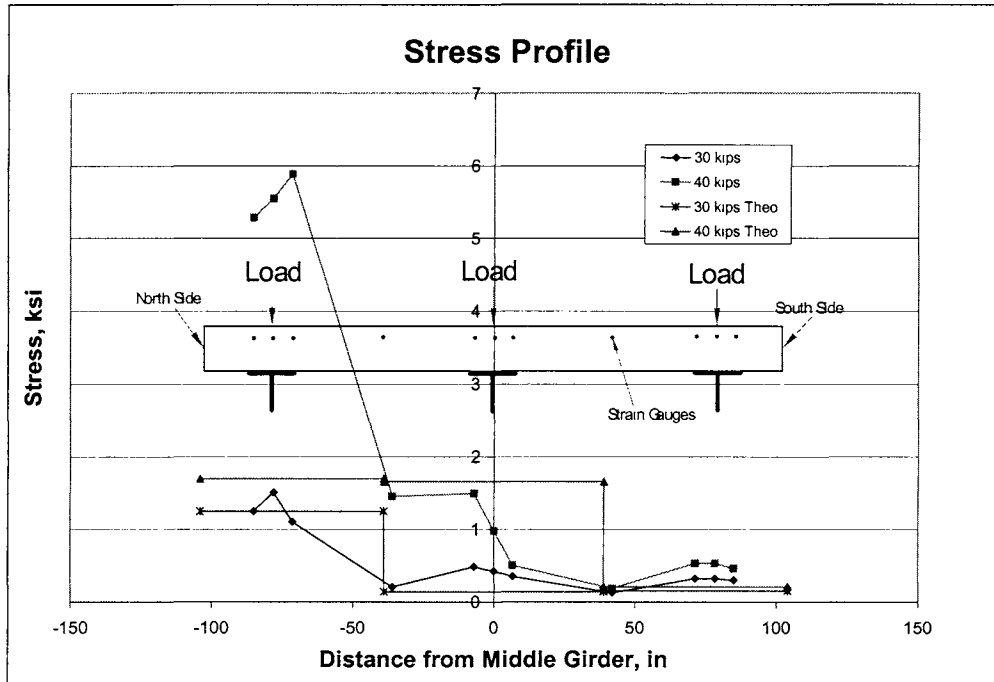


Figure 43. Stress profile for cantilever test.

Crack Widths and Cracking Loads

The first visible crack was seen at a load of 40 kips per load ram; this was the first load at which the deck was visibly inspected, so a visible crack may have occurred earlier. The first crack appeared directly over the first support spanning from the north side edge all the way to the interior girder. As the load increased, the crack progressed along the first support until it reached the south side edge of the slab. More cracks with the same pattern formed in the negative moment regions. The progression and location of these cracks can be seen in Figure 44.

As stated above, the first visible crack was seen at a load of 40 kips over the north side and interior girders. This corresponds with the girder strain data in which it was seen that the neutral axis lowered at a load of 40 kips, indicating a crack. At a load of 50 kips, the slab above the south side girder was cracked, which also corresponds to what was seen in the steel reinforcing bar, the girder, and the GFRP strain data presented previously.

The estimated cracking load was calculated by dividing the cracking moment, M_{cr} , by the moment arm of 4 ft. Equation 5 was used to calculate the cracking moment.

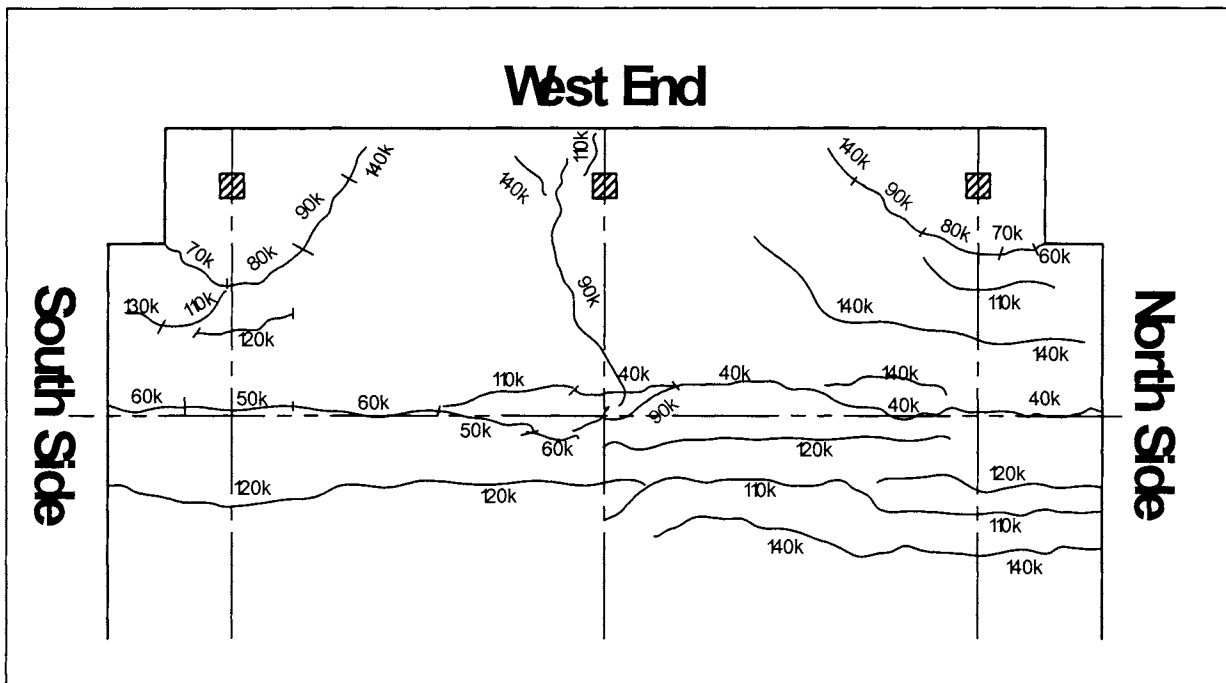


Figure 44. Crack map for cantilever test, loads shown are per load patch.

The concrete tensile strength was transformed to an equivalent steel tensile strength because the transformed moment of inertia and its corresponding y value were calculated by transforming all materials to steel. To do this, the concrete tensile strength was divided by 0.1556, the modular ratio of the concrete to the steel. A concrete compressive strength of 6,270 psi was used for the calculation because this was the average strength of batch 2 at 61 days. For

the interior girder, the cracking moment was calculated to be 443.8 ft-kips, which corresponds to a cracking load of 111 kips. For the exterior girder, the cracking moment was calculated to be 408 ft-kips, which corresponds to a cracking load of 102 kips. Both of these estimated cracking loads are considerably larger than the observed cracking load. Some reasons for this large over-prediction may be shear lag, loss of composite action between the slab and the girder, and unconservative effective flange widths, but these alone would not account for such a large error.

The measured and calculated crack widths for the interior girder test are presented in Table 11. The crack widths were measured using a crack microscope, which is much more accurate than a crack card. The crack widths were calculated using Equation 6, the ACI 440 (ACI 2001) modified Gergely-Lutz equation as shown previously.

As can be seen in Table 11, the ACI 440 equation for crack widths over-predicts the measured values, proving the equation to be extremely conservative, especially for the given cantilever situation. One interesting fact is that the equation is a function of the stress in the GFRP reinforcing bars and since the stress in the bars is being drastically under-predicted, it would be thought that the crack widths would be under-predicted as well, but they are not. Overall, this equation is very conservative and may not be suited for this particular application of a composite girder and slab.

Table 11. Measured and Calculated Crack Widths

Load, kips	Calculated Crack Width, in	Measured Crack Width, in
10	0.0079	0.0010
40	0.0301	0.0079
50	0.0379	0.0102
60	0.0463	0.0118
70	0.0534	0.0142
80	0.0610	0.0197
90	0.0689	0.0189
110	0.0835	0.0236
130	0.0992	0.0260
140	0.1055	0.0260

Design Criteria

Table 12 shows a comparison among allowable, measured, and calculated values for various design criteria. For the measured values, all measurements were taken at an approximate service load on the bridge. The service load was calculated by finding the largest negative moment on the actual bridge. The bridge was modeled as a three-span continuous structure, with each span 45 ft in length. An influence function was created for the model, and AASHTO LRFD (1998) design trucks and lane loads were placed on the model to create the largest negative moment over a support. The resulting maximum negative moment due to a truck was 272 ft-kips and due to a lane load was 150 ft-kips.

The service moment was then calculated by multiplying the moment due to the design truck by an impact factor of 1.33 and adding it to the lane load moment, giving a total service moment of 512 ft-kips. Distribution factors were then applied in accordance with AASHTO

LRFD. The distribution factor for the exterior girder was 0.621, giving it a moment of 318 ft-kips, and 0.574 for the interior girder, giving it a moment of 294 ft-kips. The prototype had two exterior and one interior girder, so the three moments were averaged to 310 ft-kips. This was divided by the moment arm of 4 ft and yielded a load of 78 kips per ram. The load was applied in 10 kip increments, so 80 kips per ram was used as the service load.

The allowable stresses were calculated in accordance with the ACI 440 (ACI 2001) guidelines. For cyclic stress limits in GFRP reinforcement, the allowable stress for the No. 6 bars is 10.6 ksi. As can be seen in the table, the measured value is greater than the allowable design value, although the calculated value is less. This indicates that the design is unconservative and the design needs to be reevaluated.

Table 12. Design Criteria for Cantilever Test

Design Criteria	Cantilever Test Values		
	Allowable	Measured	Calculated
Stresses, ksi	10.6	12.0	3.44
Crack Widths, in	0.02	0.0197	0.061
Deflections, in	0.20	0.32	0.19

The crack widths were calculated using Equation 6. The load used for the calculation was 80 kips per load patch. ACI 440 (ACI 2001) recommends a maximum crack width of 0.02 in. The calculated value is well above the measured value, indicating that the design is conservative or the equation needs to be changed. The measured crack width is approximately equal to the allowable, indicating an acceptable design.

The AASHTO LRFD Bridge Design Specifications (1998) set the recommended, not mandatory, allowable deflections at service loads of a cantilever section as the length of the cantilever section divided by 300. The cantilever test had a length of 60 in, leading to an allowable deflection of 0.2 in at a service load of 80 kips. The measured deflection of the overhang at service was 0.32 in which is above the recommended value.

CONCLUSIONS

Deflections

- *The effective moment of inertia method, used in conjunction with the AASHTO LRFD effective widths, models overhang deflections at service loads reasonably well.* For both overhangs, the two theoretical methods used accurately predicted the deflections up to a load of 30 kips for Overhang 1 and 16 kips for Overhang 2. The effective moment of inertia method was more accurate in both cases for predicting the deflections during cracking, but did not accurately predict the load at which cracking occurred. The measured deflections at service were below the recommended allowable.
- *The effective moment of inertia method, used in conjunction with the AASHTO LRFD effective widths, and the averaged moment of inertia method recommended by ACI 435 (ACI 1995) for continuous members, models slab deflections between girders at service*

loads well. For the interior girder test, the measured deflections of the slab at service were below the recommended allowable deflection.

- *Calculation of the deflection of short cantilevers by using transformed section properties for the composite girder and including the shear deformations of the steel beam results in good prediction of the deflection, but overpredicts the stiffness of the section by 30 to 50%.* The measured deflections at service were above the recommended allowable, proving the design to be unconservative in regards to deflections.

Stresses

- *Calculation of stresses in GFRP reinforcing bars at service, using cracked section properties and the AASHTO effective slab width, results in conservative predictions of rebar stresses.* Overhang Tests 1 and 2, and the interior girder test all had similar results with respect to predicted stresses as compared to measured stresses. The calculations predicted the measured stresses reasonably well at low loads before cracking occurred. Near the cracking load, the calculated stresses were somewhat smaller than the measured stresses. After cracking, the calculated stresses were considerably larger than the measured stresses and are considered to be very conservative. However, all the measured stresses were well below allowable at service loads.
- *The design of the GFRP reinforcement for the cantilever test, which mimicked a slab continuous over an interior support, was unconservative with respect to reinforcement stresses.* The measured stresses were not well predicted for the cantilever test. Before cracking, calculated stresses were slightly smaller than the measured stresses. After the section had become cracked over the full width of the deck, the calculated stresses were considerably less than the measured stresses. The stresses in the reinforcement at service were above the allowable stresses as prescribed by ACI 440 (ACI 2001).

Crack Widths

- *The deck design is conservative with respect to crack widths.* Overhang Tests 1 and 2, and the interior girder test all had similar results with respect to their predicted crack widths as compared to the actual crack widths. The calculated crack widths were considerably larger than the measured crack widths. At service load for each test, the measured crack widths were well below the ACI 440 (ACI 2001) recommended value for allowable crack widths of 0.02 in, and in all three tests, the slab was not cracked when service load was first reached. Most of the reason for this over-prediction can be attributed to the fact that the stresses used for the crack width calculation were over-predicted as well. Another contributor to the over-prediction could be the bond factor, k_b . This is an arbitrary factor that increases the theoretical crack width by 30%.
- *The cantilever section design is adequate for crack width limitations, but the method used to calculate crack widths is inadequate.* The calculated crack widths for the cantilever test were well above the actual measured values. This is surprising considering that the theoretical stresses used to calculate the crack widths were well below the measured stresses. The measured crack width at service was equal to the ACI 440 (ACI 2001) recommended allowable value.

Cracking Load

- *Neither method used to calculate first cracking load was accurate in its prediction for the overhang tests, but the moment influence surface method provided a conservative estimate.* For both overhang tests, the effective width method over-predicted the cracking load and the moment influence surface method under-predicted the cracking load.
- *The effective width method predicted the cracking load for the interior girder test quite well.* The predicted cracking load of 50 kips was very close to the observed cracking load of 60 kips. The load was applied in 10 kip increments, therefore cracking could have occurred at a load below 60 kips, but was not seen until 60 kips
- *Using transformed section properties with AASHTO effective flange widths is not adequate for predicting cracking loads due to negative moment over an interior support.* The predicted cracking load for the cantilever test was very unconservative. The section cracked at a load well below the expected load.

Failure Mode and Load

- *Both overhang tests failed at a much higher load than expected and by a different mode than expected.* Both were expected to fail in one-way shear, but both failed in two-way or punching shear. The predicted failure load for one-way shear was calculated using the ACI 440 (ACI 2001) modified equation and was very low. Even though the section did not fail in one-way shear, this equation is concluded to be too conservative. The ACI equation for the two-way shear capacity of the section predicted the failure loads relatively well, but was slightly unconservative.
- *The deck over interior girders has adequate shear strength, much higher than anticipated.* The interior girder test failed in punching shear, which was expected. The slab failed at a much higher load than expected. The same punching shear capacity equation used for the overhang tests was used for this test. The equation yielded a very conservative failure load, much lower than the actual failure load.

Validity of Deck Design

- *The deck has more than adequate strength to resist the design loads.* The only area of major concern is the higher than allowable stresses found in the reinforcement over the interior support during the cantilever test. This, however, is not a concern with the actual design because the bridge is designed as three simple spans and therefore no section is cantilevered or continuous over a support. The overhang sections were found to have more than adequate strength, and the interior girder test also proved the design to be adequate. Overall, the design is very conservative and there is no concern about failure of the GFRP reinforced deck.

Constructability

- *The only concerns with the construction were the plastic chairs used to support the bars, the flexibility and strength of the bars when stepped on by a 250 pound construction worker, and getting glass fibers in one's hands from handling the bars.* The bottom mat of steel was laid and tied first. The steel bars were very heavy and could only be moved

and lifted one or two at a time. The tying of the steel bars was quite simple. The top mat of GFRP reinforcing bars was laid second. The bars were very lightweight and were much less of a burden to carry than the steel. The placing of the GFRP bars took much less time than the steel bars because of the weight and ability to lift more at a time.

RECOMMENDATIONS

1. In the transverse design of bridge decks with GFRP as top mat reinforcement the following guidelines should be followed:
 - Design the deck as a one-way slab supported on pin supports at the location of each girder.
 - Determine the load on each 1-ft-wide section of the slab by dividing the design wheel load, times impact factor, by the effective slab width as recommended in AASHTO LRFD (1998).
 - Carry out the design for nominal moment capacity, allowable stresses in the GFRP bars and crack widths per the recommendations of ACI 440 (ACI 2001).
 - Use the ACI 440 (ACI 2001) recommended equation for calculation of one-way shear strength with caution, as it is inappropriate for deck slab design and should be re-evaluated.
 - Calculate deflections for service loads using the I_e as recommended in ACI 440 (ACI 2001).
 - Estimate cracking loads for overhangs using Pucher (1977) influence surfaces.
2. In the design of the longitudinal top slab GFRP reinforcement for decks continuous over interior supports the following guidelines should be followed:
 - Calculate the GFRP bar stresses using AASHTO effective flange widths and cracked transformed section properties, recognizing that predicted stresses will be smaller than measured.
 - Design the GFRP bars to control crack widths to ensure a conservative design.
3. In the construction of bridge decks with GFRP reinforcement, the following recommendations should be considered:
 - Use epoxy coated steel chairs to support GFRP reinforcing bars. The plastic chairs used for this project were not ideal and are not recommended to be used. Because of their bulky shape they did not fit over the bottom mat well.
 - Tie the chairs to the bottom mat of steel to prevent GFRP bars from floating. This takes a little extra time to do, but not much in comparison to the time saved in placing the lighter GFRP bars.
 - Wear gloves while handling the GFRP bars, to avoid getting the fibers in one's hands.
 - Avoid stepping on the GFRP bars as they are being tied, or only step on the bars close to where they are supported on chairs. This should be done until the mat is tied together and is not as flexible.

SUGGESTIONS FOR FURTHER RESEARCH

Because there is still relatively little known about the behavior of GFRP reinforcement for concrete, further research should be done to help optimize designs. If the design approach is not optimized, designers will not frequently use GFRP because the cost will exceed the benefits. The following areas are recommended for further research to optimize the design of bridge decks with GFRP reinforcing.

A major concern seen in the testing was the poor performance of the deck in negative moment over an interior support and the inability to predict deflections, stresses, crack widths, or cracking load. This is a key area in bridge design because more and more bridges are being designed as continuous spans to eliminate joints in the bridge. It is recommended that further research be done in this area and that methods and design procedures be developed that will ensure conservative designs and will predict behavior accurately.

It is also recommended that more research be done on crack width and one-way shear strength calculations for GFRP reinforced slabs. The current design equations appear to be extremely conservative in these areas.

More research should also be done in the area of cyclic loads on concrete slabs reinforced with GFRP reinforcement. This would be very useful in studying the behavior of the decks because an actual bridge deck receives many thousands, if not millions, of truck loads while in service. The code currently has the maximum allowable stress in the reinforcing bars set at 20% of design tensile strength under cyclic loads to avoid failure due to fatigue. However, since stresses are typically over-predicted, this could be quite conservative and does not allow the designer to use the high strength of FRP.

REFERENCES

- AASHTO (1998). *AASHTO LRFD Bridge Design Specification*, American Association of State Highway and Transportation Officials, Washington, D.C.
- ACI Committee 318 (1999). *Building Code Requirements for Structural Concrete (318-99) and Commentary (318R-99)*, American Concrete Institute, Farmington Hills, MI.
- ACI Committee 435 (1995). *Control of Deflections in Concrete Structures (435R-95)*, American Concrete Institute, Farmington Hills, MI.
- ACI Committee 440 (2001). *Guide for the Design and Construction of Concrete Reinforced with FRP Bars (440.1R-01)*, American Concrete Institute, Farmington Hills, MI.
- ASTM A370-97a (1998). *Standard Test Methods and Definitions for Mechanical Testing of Steel Products*, American Society for Testing and Materials, West Conshohocken, PA.
- Bedard, C. (1992). Composite Reinforcing Bars: Assessing Their Use in Construction. *Concrete International: Design and Construction*, Vol. 14, No. 1, pp. 55-59.

- Bradberry, T.E. (2001). FRP-Bar-Reinforced Concrete Bridge Decks. *Transportation Research Board Proceedings, 80th Annual Meeting*, TRB, Washington, D.C.
- DeFreese, J.M. (2001). Glass Fiber Reinforced Polymer Bars as the Top Mat Reinforcement for Bridge Decks. M.S. Thesis, Virginia Polytechnic Institute & State University, Blacksburg, VA.
- Khalifa, M.A., Kuska, S.S.B., and Krieger, J. (1993). Bridges Constructed Using Fiber Reinforced Plastics. *Concrete International: Design and Construction*, Vol. 15, No. 6, pp. 43-47.
- Pucher, A. (1977). *Einflussfelder Elastischer Platten – Influence Surfaces of Elastic Plates*, 5th ed. Vienna and New York: Springer-Verlag.
- RISA Technologies (1993). *Educational RISA-2D (R) Version 3.00*. New York.

**APPENDIX A
INFLUENCE SURFACE METHOD**

Calculation of Cracking Load Using Influence Surface Method

First, the cracking moment, M_{cr} per ft width of slab, is calculated using Equation (5).

$$M_{cr} = \frac{f_t I_t}{y}$$

$$f_t = 7.5\sqrt{f'_c} = 7.5\sqrt{5010} = 531.0 \text{ psi}$$

$$\Rightarrow M_{cr} = \frac{531 \text{ psi}(629.9 \text{ in}^4)}{4.31 \text{ in}} = 77,605 \text{ in} - \text{lb}$$

$$\Rightarrow 77,605 \text{ in} - \text{lb} \left(\frac{1 \text{ kip}}{1000 \text{ lb}} \right) \left(\frac{1 \text{ ft}}{12 \text{ in}} \right) = 6.47 \text{ ft} - \text{kips}$$

Next, the Pucher influence surface map, Figure A.1, is used with a 21-in cantilever length and a load located 11 in from the support. This corresponded to an influence surface value of 9.1. This is then used to calculate the cracking load, P_{cr} .

$$\frac{9.1 P_{cr}}{8\pi} = M_{cr} \Rightarrow P_{cr} = \frac{M_{cr} \cdot 8\pi}{9.1}$$

$$P_{cr} = \frac{(8\pi)6.47 \text{ ft} - \text{kips}}{9.1} = 17.9 \text{ kips}$$

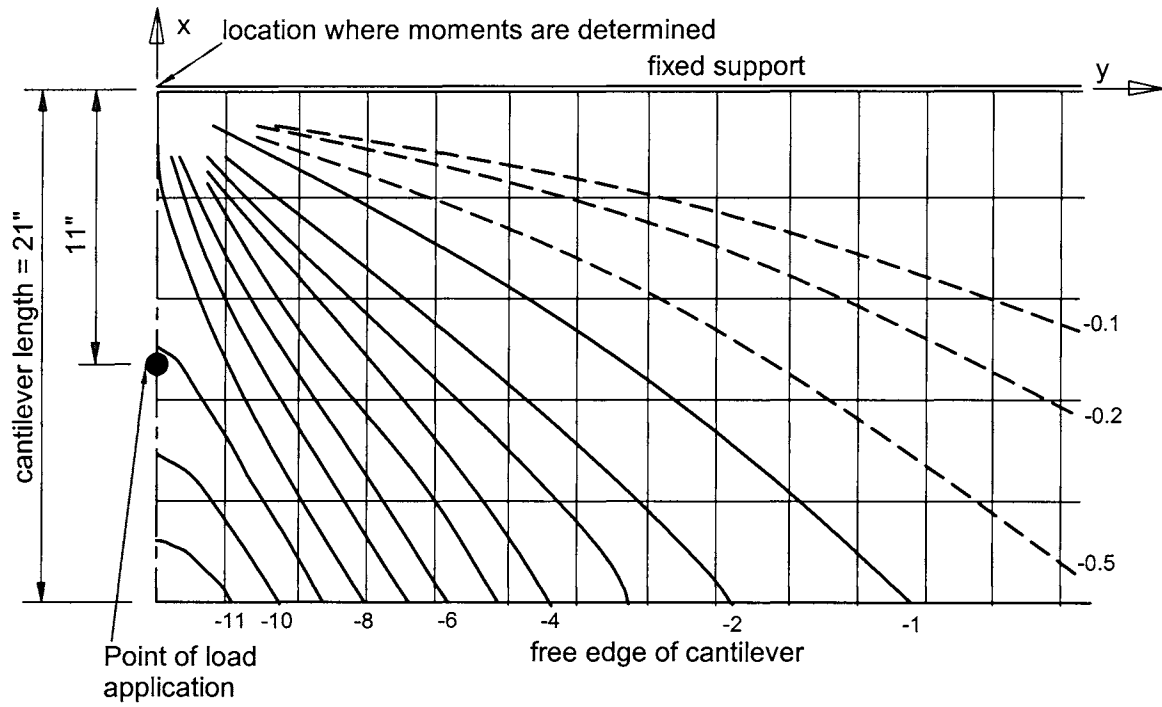


Figure A.1. Influence surface map (after Pucher (1977)) to calculate moment at support due to wheel patch load.

APPENDIX B SAMPLE CALCULATIONS

Transformed Moment of Inertia for Cantilever Test

Uncracked Section, Interior Girder

The effective flange width of the slab was calculated to be 78 in using Equation (14). The W 27x94 girder has an area of 27.7 in² and a moment of inertia, I, of 3270 in⁴. The effective width of the slab contains 13 No. 6 GFRP bars each with an area of 0.44 in² and 13 No. 4 steel bars each with an area of 0.2 in². The modulus of elasticity is 6,300 ksi for the GFRP bars and 29,000 ksi for the steel bars and the steel girder. The concrete compressive strength is 6,270 psi, corresponding to a modulus of elasticity of 4,512 ksi. The girder is 26.92 in tall, and there is a 1½ in concrete haunch on top of the girder. The slab is 7½ in thick and is on top of the haunch. The centroid of the GFRP bars is 2⁷/₈ in from the top of the slab and the centroid of the steel bars is 2 in from the bottom of the slab.

First, the areas of the concrete and GFRP are transformed into equivalent steel areas. This is done by multiplying the areas by the modular ratios of concrete to steel, n_c , and of GFRP to steel, n_f .

$$n_c = \frac{4512 \text{ ksi}}{29000 \text{ ksi}} = 0.1556; n_f = \frac{6300 \text{ ksi}}{29000 \text{ ksi}} = 0.2172$$

$$A_t = 27.7 \text{ in}^2 + 0.2 \text{ in}^2(13) + 0.1556(1.5 \text{ in} \cdot 10 \text{ in} + 78 \text{ in} \cdot 7.5 \text{ in}) + 0.2172(0.44 \text{ in}^2)(13) = 124.9 \text{ in}^2$$

Next, the location of the centroid from the bottom of the girder, c_b , is calculated.

$$C_b = \frac{27.7 \text{ in}^2(13.46 \text{ in}) + 0.2 \text{ in}^2(13)(30.42 \text{ in}) + 0.1556(1.5 \text{ in} \cdot 10 \text{ in})(27.67 \text{ in})}{124.9 \text{ in}^2} + \frac{(0.1556)(78 \text{ in} \cdot 7.5 \text{ in})(32.17 \text{ in}) + 0.2172(0.44 \text{ in}^2)(13)(33.05 \text{ in})}{124.9 \text{ in}^2} = 27.9 \text{ in}$$

Finally, the transformed moment of inertia for the section, I_t , is calculated.

$$I_t = 3270 \text{ in}^4 + 27.7 \text{ in}^2(27.9 \text{ in} - 13.46 \text{ in})^2 + 0.2 \text{ in}^2(13)(30.42 \text{ in} - 27.9 \text{ in})^2 + 0.1556(1.5 \text{ in} \cdot 10 \text{ in})(27.9 \text{ in} - 27.67 \text{ in})^2 + (0.1556)(78 \text{ in} \cdot 7.5 \text{ in})(32.17 \text{ in} - 27.9 \text{ in})^2 + 0.2172(0.44 \text{ in}^2)(13)(33.05 \text{ in} - 27.9 \text{ in})^2 + \frac{1}{12}(12.14 \text{ in})(7.5 \text{ in})^3 = 11,182 \text{ in}^4$$

Cracked Section, Interior Girder

The transformed moment of inertia for the cracked section was calculated exactly the same way as for the uncracked section. The only difference between the two was that it was assumed that absolutely no concrete was present to add strength to the cracked section.

First, the area of the GFRP was transformed into an equivalent steel area. This is done by multiplying the area by the modular ratios of GFRP to steel, n_f .

$$n_f = \frac{6300 \text{ ksi}}{29000 \text{ ksi}} = 0.2172$$

$$A_t = 27.7 \text{ in}^2 + 0.2 \text{ in}^2 (13) + 0.2172(0.44 \text{ in}^2)(13) = 31.54 \text{ in}^2$$

Next, the location of the centroid from the bottom of the girder, c_b , is calculated.

$$c_b = \frac{27.7 \text{ in}^2 (13.46 \text{ in}) + 0.2 \text{ in}^2 (13) (30.42 \text{ in}) + 0.2172 (0.44 \text{ in}^2) (13) (33.05 \text{ in})}{31.54 \text{ in}^2} = 15.63 \text{ in}$$

Finally, the cracked transformed moment of inertia for the section, I_{cr} , is calculated.

$$I_{cr} = 3270 \text{ in}^4 + 27.7 \text{ in}^2 (15.63 \text{ in} - 13.46 \text{ in})^2 + 0.2 \text{ in}^2 (13) (30.42 \text{ in} - 15.63 \text{ in})^2 + 0.2172 (0.44 \text{ in}^2) (13) (33.05 \text{ in} - 15.63 \text{ in})^2 = 4346 \text{ in}^4$$

Transformed Moment of Inertia of Overhang 1

Uncracked Section

The properties of the deck were calculated assuming the deck to be a 1-ft-wide strip in the transverse direction. The depth of the overhang portion is 8½ in. The centroid of the GFRP bars is 2³/₈ in from the top of the slab, the bars have an area of 0.93 in² per foot, and a modulus of elasticity, E_f , of 6300 ksi. The centroid of the steel bars is 6¹/₈ in from the top of the slab; the bars have an area of 0.66 in² per foot and a modulus of elasticity, E_s , of 29,000 ksi. The concrete had a compressive strength, f_c' , of 5,010 psi, corresponding to a modulus of elasticity of 4,036 ksi.

First, the areas of the steel and GFRP were transformed into equivalent concrete areas. This was done by multiplying the areas by the modular ratios of steel to concrete, n_s , and of GFRP to concrete, n_f .

$$n_s = \frac{29000ksi}{4036ksi} = 7.19$$

$$n_f = \frac{6300ksi}{4036ksi} = 1.56$$

$$A_t = 12in \cdot 8.5in + 0.93in^2(1.56 - 1) + 0.44in^2(7.19 - 1) = 106.6in^2$$

Next, the location of the centroid from the bottom of the slab, c_b , is calculated.

$$c_b = \frac{12in \cdot 8.5in \cdot 4.25in + 0.93in^2(1.56 - 1)(6.125in) + 0.44in^2(7.19 - 1)(2.375in)}{106.6in^2} = 4.19in$$

Finally, the transformed moment of inertia for the section, I_t , is calculated.

$$I_t = 12in \cdot 8.5in(4.25in - 4.19in)^2 + 0.93in^2(1.56 - 1)(6.125in - 4.19in)^2 + 0.66in^2(7.19 - 1)(4.19in - 2.375in)^2 + \left(\frac{1}{12}\right)12in(8.5in)^3 = 629.9in^4$$

Cracked Section

Everything is the same for this calculation as for the uncracked calculation, except the fact that the concrete is now cracked. In order to calculate the cracked moment of inertia, I_{cr} , for the section, the centroid must first be located. The centroid is assumed to be below the steel reinforcement, and its location is measured to be a distance, c , from the bottom of the slab. This assumption presumes that the steel is in tension after the section becomes cracked. To find the location of the centroid, c , the moment of area about the centroid due to tension is set equal to the moment of area about the centroid due to compression, and c is solved for:

$$12in \cdot c \left(\frac{c}{2}\right) = 0.66in^2(7.19)(2.375in - c) + 0.93in^2(1.56)(6.125in - c)$$

$$\Rightarrow c^2 + 1.033c - 3.36c = 0$$

$$\Rightarrow c = 1.39in$$

This proves the assumption of the centroid being below the steel correct. Finally, the cracked moment of inertia, I_{cr} , is calculated.

$$I_{cr} = \left(\frac{1}{12}\right)12in(1.39in)^3 + 12in \cdot 1.39in(0.695in)^2 + 0.93in^2(1.56)(6.125in - 1.39in)^2 + 0.66in^2(7.19)(2.375in - 1.39in)^2 = 47.9in^4$$